

**MATHEMATICAL MODELING OF PEM FUEL CELL CATHODES:
COMPARISON OF FIRST-ORDER AND HALF-ORDER
REACTION KINETICS**

by

David Castagne

A thesis submitted to the Department of Chemical Engineering

In conformity with the requirements for

the degree of Master of Science (Engineering)

Queen's University

Kingston, Ontario, Canada

(September, 2008)

Copyright ©David Castagne, 2008

Abstract

Mathematical modeling helps researchers to understand the transport and kinetic phenomena within fuel cells and their effects on fuel cell performance that may not be evident from experimental work. In this thesis, a 2-D steady-state cathode model of a proton-exchange-membrane fuel cell (PEMFC) is developed. The kinetics of the cathode half-reaction were investigated, specifically the reaction order with respect to oxygen concentration. It is unknown whether this reaction order is one or one half. First- and half-order reaction models were simulated and their influence on the predicted fuel cell performance was examined. At low overpotentials near 0.3 V, the half-order model predicted smaller current densities (approximately half that of the first-order model). At higher overpotentials above 0.5 V, the predicted current density of the half-order model is slightly higher than that of the first-order model. The effect of oxygen concentration at the channel/porous transport layer boundary was also simulated and it was shown the predicted current density of the first-order model experienced a larger decrease (~10-15% difference at low overpotentials) than the half-order model.

Several other phenomena in the cathode model were also examined. The kinetic parameters (exchange current density and cathode transfer coefficient) were adjusted to assume a single Tafel slope, rather than a double Tafel slope, resulting in a significant improvement in the predicted fuel cell performance. Anisotropic electronic conductivities and mass diffusivities were added to cathode model so that the anisotropic structure of the porous transport layer was taken into account. As expected, the simulations showed improved performance at low current densities due to a higher electronic conductivity in the in-plane direction and decreased performance at high current densities due to smaller diffusivities. Additionally, the concentration overpotential was accounted for in the model; however it had little influence on the simulation results.

Acknowledgements

I would like to thank Dr. Kim McAuley and Dr. Kunal Karan of Queen's University and Dr. Steve Beale of NRC for their excellent supervision on this research project. I also appreciate the support I received from FCRC and those working there.

I would also like to acknowledge the financial support of OGS and the School of Graduate Studies.

Table of Contents

Abstract	ii
Acknowledgements	iii
Table of Contents	iv
List of Figures	vi
List of Tables.....	viii
List of Symbols	ix
Chapter 1 Introduction	1
1.1 Background	1
1.2 Objectives.....	5
1.3 Thesis Outline	5
Chapter 2 Literature Review and Background Information.....	7
2.1 Introduction.....	7
2.2 PEMFC Cathode Models	7
2.3 Oxygen Reduction Reaction (ORR) Order with Respect to Oxygen	9
2.4 Tafel Slope Kinetics	11
2.5 Anisotropy of the PTL.....	14
2.5.1 Conductivity	14
Chapter 3 Cathode Model	18
3.1 Introduction	18
3.2 Model Description.....	18
3.2.1 Physical and Chemical Phenomena Considered.....	18
3.2.2 Model Domain.....	22
3.2.3 Model Assumptions.....	23
3.2.4 Transport and Reaction Modeling.....	24
3.3 Model Equations and Boundary Conditions	28
3.3.1 Model Equations	28
3.3.2 Boundary Conditions.....	30
3.3.3 Model Parameters.....	31
3.4 Solution Method.....	36
3.4.1 Mesh Matrix Used for Numerical Solution.....	37
3.5 Results and Discussion.....	38
3.5.1 Additional Considerations.....	42

3.5.2 Grid Study	47
3.6 Error Analysis	52
Chapter 4	57
4.1 Background	57
4.2 Thiele Modulus for Half-Order Reaction	58
4.3 Effectiveness Factor	59
4.4 The Oxygen Surface Concentration at the ionomer film inner interface	60
4.5 Reaction Rate at the Catalyst Surface	62
4.6 Kinetic Influence on Cathode Performance	63
4.7 Solution Method (Half-order Reaction)	64
4.8 Results and Discussion.....	66
4.9 Results and discussion for first and half-order models under varying oxygen concentrations	71
Chapter 5	78
5.1 Conclusions	78
5.2 Recommendations	81
Appendix A	88
Table A.2: Stationary solver settings	88
Table A.3: Parametric solver settings.....	89
Table A.4: Model adaptive mesh settings	89
Appendix B	90

List of Figures

1.1	TEM micrograph of platinum/carbon catalyst in a PEMFC	3
2.1	Reaction order plot for a microelectrode using air at 50°C.....	11
2.2	Tafel plot for oxygen reduction reaction on a microelectrode using air at 50°C.....	13
2.3	A SEM image of a typical carbon paper used in a PEMFC. a) view of through-plane b) view of in-plane.....	14
3.1	2-D diagram of cathode domain.....	20
3.2	Domain of 2-D cathode model. Agglomerate is shown with intersitial and surrounding ionomer film.....	22
3.3	Mesh Geometry of a) Coarse Mesh b) Fine Mesh c) Adaptive Mesh use in the base case model.....	40
3.4	Predicted polarization curve of the 2-D steady-state cathode model base case.....	41
3.5	The current density distribution (A/cm^2) between the catalyst layer and membrane at a NCO of a) 0.3V b) 0.5V c) 0.65V.....	42
3.6	Predicted polarization curves comparing each additional change made to the original model.....	44
3.7	Current density plot at an NCO of 0.5 V. Curves are presented comparing each additional change made to the original model.....	46
3.8	The current density distribution (A/cm^2) between the catalyst layer and membrane at a NCO of a) 0.3V b) 0.5. c) 0.7 for three mesh cases, a base case of ~6000 elements, a finer mesh case of ~14000 elements and a final case at ~16000 elements.....	50
3.9	The current density distribution (A/cm^2) between the catalyst layer and membrane at a NCO of a) 0.3V b) 0.5. c) 0.7 for two adaptive mesh cases, a coarse case of 8000 to 9500 elements, a fine case of 10500 to 13500 elements.....	51
3.10	The current density distribution (A/cm^2) between the catalyst layer and membrane at a NCO of 0.5 V. A base case is shown using an adaptive mesh, as well two additional cases where the initial guess of the concentrations and potentials are changed.....	54
3.11	Residual plot of oxygen concentration at an NCO of 0.30 V for an adaptive mesh. Residuals range from $-1.426e^{-19}$ to $1.619 e^{-19}$	56
4.1	Effectiveness factor vs. Thiele Modulus for a half-order reaction.....	60
4.2	A comparison of the current density distribution using the Tafel equation for cell potentials between 0.3 and 1.1 V.....	64
4.3	Predicted polarization curves of the PEMFC cathode model for cases where a first-order and half-order reaction is assumed.....	67
4.4	The current density distribution (A/cm^2) between the catalyst layer and membrane at a NCO of a) 0.3V b) 0.5. c) 0.7 Cases for a first-order and half-order reaction are presented.....	68
4.5	The oxygen reaction rate profile ($\text{mol}/\text{m}^3/\text{s}$) in the catalyst layer for a NCO of a) 0.3V b) 0.5V c) 0.70V. Cases for a first-order and half-order reaction are presented.....	70
4.6	Predicted polarization curves of the PEMFC cathode model for the first-order reaction. Three cases are considered where the oxygen concentration at the channel/PTL boundary is varied, case 1 ($9.18 \text{ mol}/\text{m}^3$), case 2 ($6.99 \text{ mol}/\text{m}^3$) and case 3 ($4.18 \text{ mol}/\text{m}^3$).....	74
4.7	Predicted polarization curves of the PEMFC cathode model for the half-order reaction. Three cases are considered where the oxygen concentration at the channel/PTL boundary is varied, case 1 ($9.18 \text{ mol}/\text{m}^3$), case 2 ($6.99 \text{ mol}/\text{m}^3$) and case 3 ($4.18 \text{ mol}/\text{m}^3$).....	74
4.8	Dissolved oxygen concentration at the inside of the ionomer interface, $\text{CO}_2, \text{l/s}$ at the PTL / CL interface.....	75

4.9	Predicted polarization curves of the PEMFC cathode model for case 2 (6.99 mol/m ³ O ₂ concentration). First- and half-order cases are considered.....	77
4.10	Predicted polarization curves of the PEMFC cathode model for case 3 (4.18 mol/m ³ O ₂ concentration). First- and half-order cases are considered.....	77

List of Tables

3.1	Summary of transport equations for chemical, electronic and ionic species.....	28
3.2	Summary of source terms, boundary for each domain. Boundary conditions for the gaseous species are given in mass fractions.....	29
3.3	Operating conditions considered for the model.....	31
3.4	Model Parameters.....	32
3.5	Number of elements in each manually-generated mesh case.....	49
3.6	Material balances on chemical, electronic and ionic species. The flux through four separate boundaries of the domain is given.....	55
4.1	Chemical species concentrations at the channel/PTL boundary for case 1 (base case), case 2 (mid-oxygen concentration) and case 3 (low oxygen concentration).....	71
4.2	Relative decrease in current density of case 2 and 3 in comparison to the base case for the first- and half-order reaction models.....	72
A.1	Model solver settings.....	88
A.2	Stationary solver settings.....	88
A.3	Parametric solver settings.....	89
A.4	Model adaptive mesh settings.....	89

List of Symbols

a_{agg}	Agglomerate surface area per unit volume of catalyst, m^2/m^3
a_{pt}	Theoretical platinum loading surface, m^2/m^3
$a_{\text{Pt}}^{\text{eff}}$	Effective platinum specific surface area, m^2/m^3
C_{O_2}	Dissolved oxygen concentration in the an agglomerate, mol/m^3
$C_{\text{O}_2}^{\text{ref}}$	Reference oxygen concentration, mol/m^3
$C_{\text{O}_2,\text{g/l}}$	Oxygen concentration at the ionomer film surface, mol/m^3
$C_{\text{O}_2,\text{l/s}}$	Oxygen concentration at the agglomerate surface, mol/m^3
c_i	Concentration of species i, mol/m^3
D	Diffusion coefficient of dissolved oxygen in the ionomer, m^2/s
D^{eff}	Effective diffusion coefficient of dissolved oxygen in ionomer, m^2/s
D_{ij}	Binary diffusion coefficients of i through j, m^2/s
D_{im}	Diffusion coefficient of species i through the gas mixture, m^2/s
D_{im}^{eff}	Effective diffusion coefficient of species i through the gas mixture, m^2/s
E_r	Effectiveness factor
ΔE_{exc}	Activation energy of the ORR, kJ/mol
E_{rev}	Reversible cell potential, V
e^-	Electron
F	Faraday's Constant
f_{Pt}	Effective platinum surface ratio
H	Henry's law constant for oxygen dissolved in ionomer, $\text{atm m}^3/\text{mol}$
H_2	Hydrogen
H^+	Hydrogen ion
H_2O	Water
i	Local current density, A/cm^2
i_0	Exchange current density (per unit area of the CL), A/cm^2
i_0^{ref}	Reference exchange current density at reference oxygen concentration (per unit area of platinum surface area in the CL), A/cm^2
$j_{i,C}$	Molar flux of species i through the catalyst layer, $\text{mol}/(\text{m}^2 \text{ s})$
$j_{i,P}$	Molar flux of species i through the PTL, $\text{mol}/(\text{m}^2 \text{ s})$

k_c	Reaction rate constant, 1/s (first-order)
k_e	Electronic conductivity, S/m
k_e	Electronic conductivity, S/m
k_e^{eff}	Effective electronic conductivity, S/m
k_p	Ionic conductivity, S/m
k_p^{eff}	Effective ionic conductivity, S/m
M	Molecular weight of the gas mixture, kg/mol
m_{Pt}	Platinum loading, kg/m ²
O_2	Oxygen
P	Total pressure, atm
P_{O_2}	Oxygen partial pressure, atm
Pt	Platinum
R	Gas consant, J/(mol K)
R_{O_2}	Oxygen reaction rate per unit catalyst layer volume, mol/(m ³ s)
RH	Relative Humidity
r_{agg}	Radius of agglomerate, m
$S_{i,C}$	Source term of species i through the CL
$S_{i,P}$	Source term of species i through the PTL
S_{ac}	Platinum surface area per unit mass, m ² /kg
T	Operating temperature of fuel cell, °C
t_{cl}	Catalyst thickness, m
V_c	Actual cell voltage, V
w_i	Mass fraction of species i
x_i	Mole fraction of species i
x_0	Left boundary wall of cathode
x_{GC}	Boundary that separates the channel and the land areas
x_L	Right boundary wall of cathode
z_{CL}	PCL/CL interface
z_{PTL}	PTL/land and channel interface
z_0	CL/membrane interface

Greek Symbols

α	Net water drag coefficient
α_c	Cathode transfer coefficient
δ	Ionomer film thickness, nm
η_{act}	Activation losses, V
η_{conc}	Concentration losses, V
η_{local}	Local activation overpotential, V
η_{ohm}	Ohmic losses, V
γ	Reaction order
Φ_L	Thiele Modulus
$\phi_{e,local}$	Local electronic potential, V
$\phi_{p,local}$	Local ionic potential, V
ε_{agg}	Volume fraction of ionomer in aggregates
ε_p	Porosity of the PTL
ε_{CAT}	Porosity of the catalyst layer
λ	Water content of membrane

Subscripts

C	Catalyst Layer
e	electronic
P	PTL
p	ionic
O ₂	Oxygen
H ₂ O	Water
N ₂	Nitrogen

Abbreviations

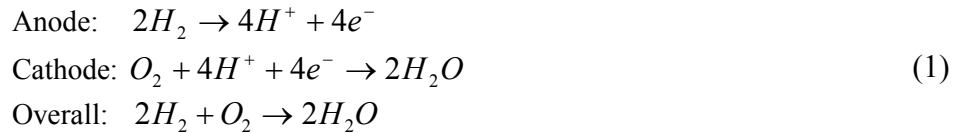
CL	Catalyst layer
ORR	Oxygen reduction reaction
NCO	Nominal cathode overpotential
PEMFC	Proton-exchange membrane fuel cell
PTL	Porous transport layer
SEM	Scanning electron microscope
TEM	Transmission electron microscope

Chapter 1

Introduction

1.1 Background

Polymer electrolyte membrane fuel cells (PEMFCs) are low-temperature fuel cells that produce electricity from hydrogen fuel and oxygen through two electrochemical half-reactions shown in Eq. (1) below.



Significant improvement in durability, cost and electrochemical behavior is still necessary to commercialize this technologically viable system. Development of strategies to improve performance while simultaneously reducing the cost is complicated. This is due to the occurrence of, and coupling between, various transport and reaction processes, which are further, influenced by PEMFC sub-component material and microstructure. Furthermore, the micro-scale phenomena are not easy to investigate in-situ. Mathematical modeling of PEMFCs allows investigation of the effects of operating conditions and sub-component material and microstructural properties on fuel cell performance. It is essential that mathematical models constructed to gain insight are accurate and reliable.

A fuel-cell stack is typically composed of 50 to 100 cells in series. Each cell includes several functionally and materially distinct sub-components. Bipolar plates connect the cells that are electrically in series (hydraulically in parallel), and provide a medium for the transport of electrons and reactant gases required for the half-reactions. The half-reactions occur at the

cathode and anode, which are separated by an ionomer membrane. Hydrogen gas is fed to the anode where it dissociates into hydrogen ions (protons) and electrons at the catalyst sites. At the cathode, oxygen gas and electrons react with the protons that have been transported from the anode through the ionomer membrane to produce water. The membrane that separates the cathode and anode is composed of a polymeric material, that when saturated with water, has a high ionic conductivity but low permeability to hydrogen and oxygen gases. Although some of the water that is produced at the cathode can diffuse through the ionomer membrane, the majority of the water passes through pores in a porous transport layer (PTL), which is adjacent to the catalyst layer, and then exits the fuel cell via channels in the bipolar plate.

The cathode half reaction is the slower of the two reactions and the electrochemical performance of a fuel cell is usually limited by the cathode processes at operating conditions of interest. As well, water accumulation can occur at the cathode, which may cause the fuel cell to flood, impeding the transport of oxygen to the catalyst sites. Hence, much research has been focused on the cathode in a PEMFC, though other components of the fuel cell are still important to consider.

It is essential that the cathode models are representative of the processes occurring therein, so that meaningful simulation results can be extracted for the design and optimization of PEMFC components. Models should be continually updated to reflect the most recent available information. The catalyst layer was modeled in a simplified manner in the earlier models (e.g. Bernardi and Verbrugge, 1991, Springer *et al.*, 1991). For example, the catalyst layer (CL) has been treated as an ultra-thin layer, with sink and source terms that model the electrochemical reactions. However, the mass transport of reactants and products inside the catalyst cannot be modeled by assuming an ultra-thin catalyst layer. Further improvements led to the development

of homogeneous flooded models, wherein the catalyst layer is considered to be of finite thickness as well the CL composition - carbon particles, platinum catalyst and porous regions filled with water-saturated ionomer - are included. Mass transport inside the catalyst layer is also modeled, but the microstructure of the catalyst layer is not considered. Recently, scanning electron microscope (SEM) and transmission electron microscope (TEM) images (see Fig. 1.1) have shown that the catalyst layer is composed of Pt/C particles held together and surrounded by a film of ionomer, called agglomerates. The half-reaction occurs at the interface between ionomer and Pt/C particles within these agglomerates. Estimated sizes of agglomerates have ranged between

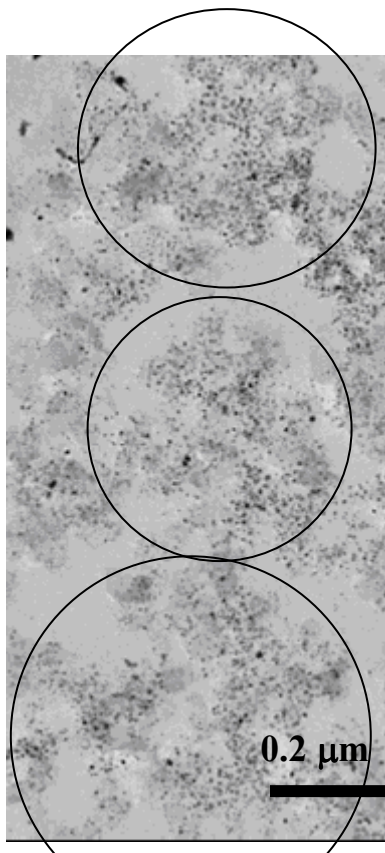


Figure 1.1: TEM image of catalyst layer. The cathode catalyst is shown in the right. The darker areas are platinum-covered carbon support and the lighter areas are ionomer electrolyte and void space {Source: More (2006)}. The circles have been added to show the dimensions of idealized agglomerates, which are used to represent the structure of the catalyst layer in this thesis.

0.5 μm (Jaouen *et al.*, 2002) to 3 μm (Siegel *et al.*, 2003). For reference, the catalyst layer has been estimated to be 15 μm in width (Broka and Ekdunge, 1997). The process used to create the catalyst layer will influence the size of the agglomerates. Sample agglomerates is shown in Fig. 1.1 and is near the size reported by Jaoen *et al.*, 2002. In case of the cathode, diffusion of oxygen through the ionomer film and its consumption at the reaction sites in the agglomerate has been modeled in past (e.g., Sun *et al.* (2005a)). Such an agglomerate model, which is more detailed than the ultra-thin catalyst model and homogeneous flooded models, provides insight into reaction rates, concentrations of reacting species and potentials inside in the catalyst layer, and microstructural parameters (agglomerate size, porosity, ionomer thickness) and their effect on fuel cell performance.

Although details of the mass transport within the catalyst layer have been included in Sun's model, questions still remain about the kinetics of the oxygen-reduction reaction (ORR). Most agglomerate models assume that the reaction order of the cathode half-cell reaction is *one* with respect to the oxygen concentration. Many of the kinetic parameters in the agglomerate model are based on kinetic data reported by Parthasarathy *et al.* (1992a, 1992b) arising from measurements conducted in a PEMFC microelectrode setup. In Parthasarathy's work, the reaction order with respect to oxygen concentration was determined to be one (calculated from the slope of logarithm of exchange current density plotted against the logarithm of oxygen partial pressure). More recently, however, Neyerlin *et al.* (2006) extracted kinetic parameters for the ORR using a combined kinetic-thermodynamic model. The parameters were simultaneously fit to their model using a set of experiments designed and run on a single-cell PEMFC unit. The reaction order for the ORR was determined to be *one half* with respect to oxygen partial pressure. These new results are significantly different than previous studies (Parthasarathy *et al.* 1992a, 1992b), where

the reaction order was found to be *one*. It is anticipated that further studies and investigations will attempt to resolve the discrepancy between these published reaction orders.

1.2 Objectives

Key objectives of this thesis are to implement half-order (with respect to oxygen) kinetics into the catalyst layer model and to investigate the influence of the reaction order and associated kinetics on the predicted electrochemical performance of the PEMFC cathode. Secondary objectives are to develop an improved 2D steady-state cathode model, based on an agglomerate representation of catalyst layer that offers several improvements compared with a previous model (Sun *et al.* 2005a). This model by Sun *et al.* is used because an agglomerate model can account for complex transport and kinetic phenomena that occur in the catalyst layer. The improved model, which accounts for concentration polarization effects and for anisotropic properties of the PTL, is used to compare predicted fuel cell behaviour using half- and first-order kinetics under a variety of operating conditions.

1.3 Thesis Outline

In Chapter 2, a short literature review of recent PEMFC models is presented. In Chapter 3, a 2D steady-state cathode model is developed, using the agglomerate model of Sun *et al.* (2005a) as a starting point. Several assumptions in Sun's model are examined in detail. Issues surrounding the Tafel slope (Perry *et al.*, 1998 and Neyerlin *et al.*, 2006) and the contribution of mass transport losses to the Butler-Volmer equation are considered, and the effects of anisotropy in the PTL are implemented in the revised model. The resulting isothermal model accounts for electron, proton, oxygen and water transport in the catalyst layer and in the PTL and predicts the reaction rates and current density profiles inside the catalyst layer. Like many other cathode models, the

model assumes that the temperature is always above the dew point of the gas mixture, so that liquid water can be neglected. An error study and mesh analysis are conducted to verify the numerical accuracy of the model predictions, which were obtained using COMSOLTM, the finite-elements package that was used to solve the model's partial differential equations. In Chapter 4, the model is modified assuming half-order reaction kinetics. Predictions from first-order and half-order models are compared to determine the consequences of changing the oxygen reaction order. Conclusions and Recommendations are presented in Chapter 5.

Chapter 2

Literature Review and Background Information

2.1 Introduction

A brief review of the catalysts layer models is presented in this Chapter. Models have advanced from originally treating the catalyst layer as an infinitely thin boundary to current agglomerate models where detailed physical characteristics of the catalyst layer are accounted for throughout the thickness of the catalyst layer. Background on the kinetics of the cathode half-reaction is also discussed, specifically the current debate on whether the (ORR) is first or half-order with respect to oxygen. As well, information on the Tafel slope kinetics and the anisotropy of the PTL is given.

2.2 PEMFC Cathode Models

There has been considerable research focused on PEMFC modeling in recent years. Sun *et al.* (2005a) completed an extensive literature review that covered various 1D, 2D and 3D models. These models consider the catalyst layer (CL) with varying levels of complexity describing the CL, with sub-models as ultra-thin layer, thin-layer flooded and agglomerate models. More recently, Madhusudana *et al.* (2007) presented a detailed review describing the several types of catalyst layer models and their development over the past 15 years. Ultra-thin-film models represent the catalyst layer as a boundary where source and sink terms are implemented to describe the electrochemical reactions. Springer *et al.* (1991) and Fuller and Newman (1993) were among the first to utilize this approach. The disadvantage of such a model is that transport phenomena inside the catalyst pores and ionomer are ignored, so that model predictions from

ultra-thin models may not be valid, particularly when mass-transfer phenomena within the catalyst influence reaction rates.

Thin-layer or homogeneous flooded models include more detail about the catalyst layer. The layer is assumed to be composed of carbon particles, catalyst and a porous region, filled with ionomer that is saturated with water. Bernardi and Verbrugge (1991) proposed this idea in a 1D cathode model, which included the ionomer membrane. Springer *et al.* (1993) also examined a flooded homogeneous model that improved upon a previous model. The reacting species and their fractions inside the catalyst layer, as well as the transport of individual species within the layer are considered in this type of model. This is an improvement upon the ultra-thin model where such details are ignored, however the detailed geometry inside the catalyst layer is not considered. The catalyst and ionomer are assumed to be distributed uniformly in the layer. As well, gaseous transport through the catalyst layer is not included, since the region is assumed to be fully-flooded. Recent evidence (SEM/TEM images, including Fig. 1.1) has suggested that this is not the case, leading to the development of agglomerate models.

The agglomerate model is currently thought to be the most detailed physical representation of the cathode catalyst layer in a PEMFC. In recent years, SEM and TEM images of the CL have shown it to consist of platinum-covered carbon particles that are *agglomerated* and surrounded by a thin ionomer film. Middleman (2002), Seigel *et al.* (2003) and, recently, More *et al.* (2006) (see Fig. 1.1) have provided electron micrographs of the catalyst layer with sub-micron scale resolution. Jaouen *et al.* (2003) created a model with spherical agglomerates to examine mass transport in the catalyst layer. However, they neglected to include electron transport. A 2D steady-state agglomerate model was proposed by Siegel *et al.* (2003), which considered the

influence of the catalyst structure on fuel cell performance. They found that key parameters, such as, void and ionomer fraction of the catalyst layer and catalyst particle geometry has a significant effect on fuel cell performance. Wang *et al.* (2004) examined both transport and reaction kinetics in their PEMFC agglomerate model. They also compared models that assumed either ionomer or water-filled agglomerates. The ionomer-filled cases generally produced more uniform reaction rate distributions within the agglomerate. Recently, Madhusudana *et al.* (2007) included liquid water transport in their 2D agglomerate model, a feature that is absent from most models. In the porous regions of the fuel cell (catalyst layer, PTL), liquid water was modeled using Darcy's law, where capillary forces drive transport. As well, the agglomerates in the catalyst layer were assumed to be surrounded by a film of water, providing an additional form of resistance to oxygen. Madhusudana concluded that modeling liquid water allows for the most accurate prediction of PEMFC polarization curves. Like most other modelers, Madhusdana *et al.* (2007) assumed that the ORR was first-order with respect to oxygen concentration.

2.3 Oxygen Reduction Reaction (ORR) Order with Respect to Oxygen

The ORR rate in PEMFCs is usually assumed to be first-order with respect to the oxygen concentration, indicating that the rate of oxygen consumption (and the current density) is proportional to the oxygen concentration at the catalyst sites. The reaction order is obtained by plotting the logarithm of the exchange current density versus the logarithm of the oxygen partial pressure. A Tafel plot is required to determine the exchange current density, i_0 , which is the intercept where the potential is extrapolated to zero. Based on this method, Parthasarathy *et al.* (1992a) determined the reaction order to be one at the platinum/nafion interface, see Fig. 2.1. This result was consistent with previous experiments (Damjanovic and Brusic, 1967 and Hsueh *et al.*, 1985) that measured the reaction order at various other platinum/liquid-acid-electrolyte

interfaces, such as HClO_4 and H_2SO_4 . PEMFC modelers, *e.g.* Wang *et al.* (2004), Sun *et al.* (2005a), and Mudhusudana *et al.* (2007), have since used a reaction order of one in their models, based on these results. Recently, Neyerlin *et al.* (2006) developed a combined thermodynamic and kinetic model to extract various kinetic parameters, such as the current density and the reaction order. They devised a set of experiments that were performed on an operating PEMFC and used measurements of current density and cell resistances to fit the parameters of their model. The reaction order was found to be approximately one half. A half-order reaction means that the rate of oxygen consumption (and the current density) depend on the oxygen concentration to the $\frac{1}{2}$ power, so that the local oxygen concentration is not as influential in determining current density as it would be for a first-order reaction. In this thesis, the first-order cathode model will be extended to accommodate half-order ORR kinetics, so that the consequences of a possible half-order reaction can be examined. The modeling results will hopefully provide clues to experimentalists who seek to resolve the controversy about the reaction order and its importance.

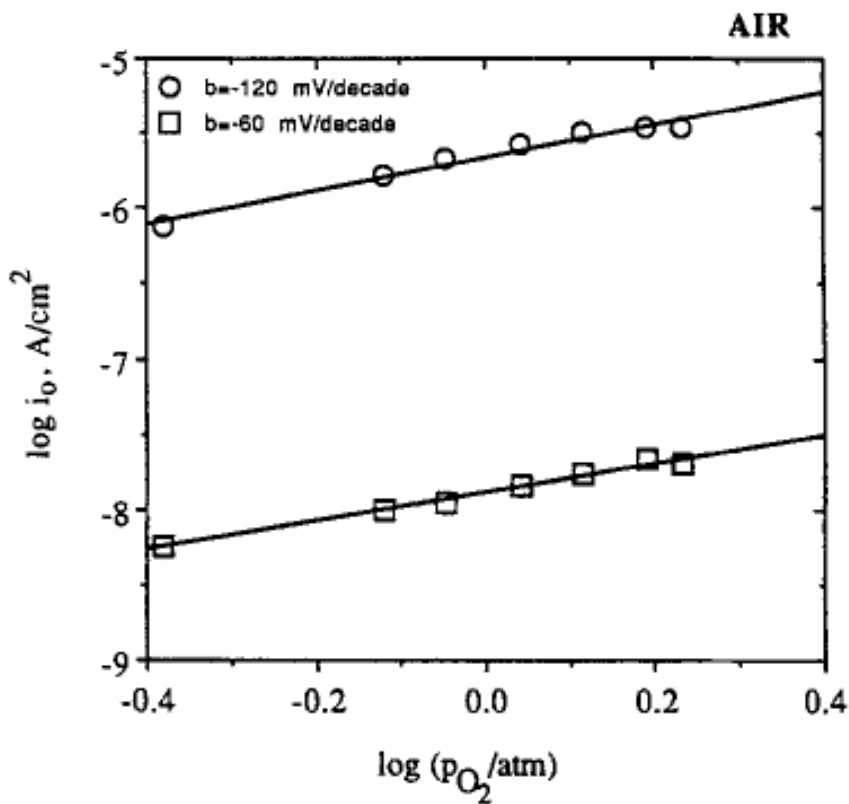


Figure 2.1: Reaction order plot from Parathasarthy et al. (1992a) for a microelectrode using air at 50°C. Both Tafel plot regions are shown.

2.4 Tafel Slope Kinetics

A Tafel plot is a graph depicting the overpotential plotted against the logarithm of the current density. A Tafel plot is useful for determining kinetic parameters, such as the exchange current density, i_0 , and cathodic transfer coefficient, α_c . The exchange current density is specific to a given catalyst/ionomer system and also depends on the operating conditions such as the temperature and pressure. i_0 is equal to the forward and the reverse current densities (which are equal in magnitude but of opposing signs) at open circuit voltage (i.e., i_0 is determined by the forward and reverse reaction rates at equilibrium). The cathodic transfer-coefficient is the portion of applied energy (overpotential) that is used to change the rate of the reaction.

The parameter α_c is obtained from the slope of the Tafel plot and i_0 from the intercept (i.e., where the cell voltage is zero). However, it has been observed that the slope of the Tafel plot changes based on the overpotential, and two distinct slopes arise. Parthasarathy *et al.* (1992a, 1992b) observed this phenomenon in a series of experiments completed with a PEMFC microelectrode setup, as shown in Fig. 2.2.

To account for the double Tafel slope, Sun *et al.* (2005a) in their cathode model used two separate α_c values, one below 0.8 V and one above. In the low slope region above 0.8 V (or below a NCO of 0.35 V), α_c and i_0 were set at 1.0 and $3.85e^{-4}$ A/cm², respectively. Above a NCO of 0.35V, the high slope region of a Tafel slope, the value of i_0 was set at 0.015 A/cm². The transfer coefficient α_c was calculated as a function of temperature, using an empirical relationship developed by Parthasarathy *et al.* (1992b).

$$\alpha_c = 0.495 + 2.3 \times 10^{-3}(T - 300) \quad (2)$$

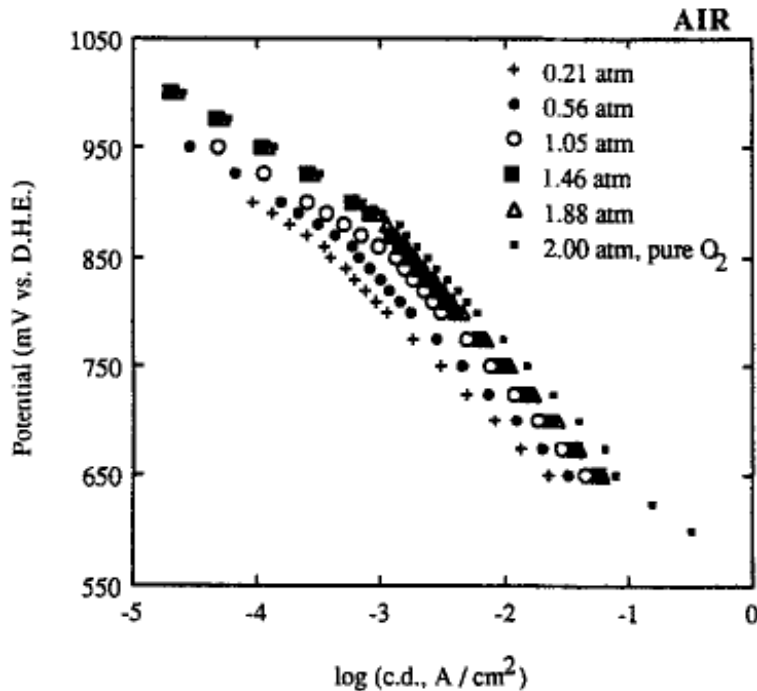


Figure 2.2: Tafel plot for oxygen reduction reaction on a microelectrode using air at 50°C {Source: Parthasarathy *et al.* (1992a)}.

Other researchers, for example Murthi *et al.* (2004) and Paulus *et al.* (2002) have reported this double Tafel slope in their rotating-disk electrode (RDEs) experiments. In general, the transition between the two slopes is at a cell voltage near 0.8 V. The transition is sometimes not well defined, and as in the case of Paulus *et al.* (2002) where the Tafel slope appears curved. However, the correction to the kinetic parameters may be unnecessary, and it has been argued that the shift in Tafel slope is due to an artifact of the experimental setup, rather than a change in the reaction kinetics. Perry *et al.* (1998) modeled coupled reaction-transport for the ORR in microelectrodes and showed that the double slope can arise from mass-transport limitations of either the oxygen gas or the ionic species in the catalyst layer. Neyerlin *et al.* (2006) arrived at the same conclusion and used a single value of α_c in their model. They believed the double slope

arises in experiments with RDEs or PEMFCs with poorly designed electrodes. In Chapters 3 and 4 of this thesis, PEMFC simulations are conducted using a single value of α_c , and the corresponding exchange current density i_0 .

2.5 Anisotropy of the PTL

2.5.1 Conductivity

In PEMFCs, the PTL is a porous carbon layer that distributes both the electrons and gases (oxygen, nitrogen and water vapour) and provides support for the catalyst layer. Typically, the carbon layer is designed as a thin woven cloth or paper structure. In the past, researchers have assumed the PTL structure to be isotropic in their models; however this is not the case. The carbon fibers are stacked in layers and the total electrical resistance is much greater in the through-plane direction. Fig. 2.3 illustrates the anisotropy that exists in a PTL. Barbir (2005)

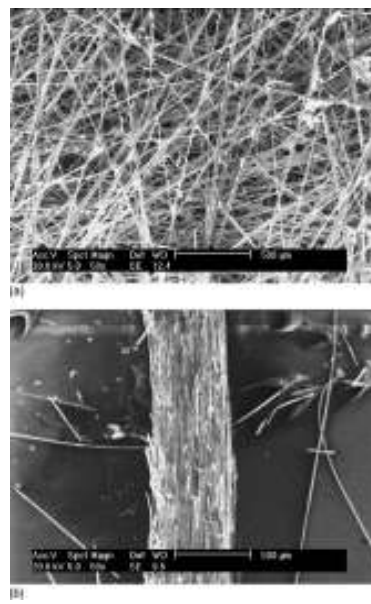


Figure 2.3: A SEM image of a typical carbon paper used in a PEMFC. a) view of through-plane b) view of in-plane (Pharoah et. al. 2006).

published electronic conductivity data for a wide variety of PTLs. The range of conductivities in the through-plane direction was 15-1250 S/m and the in-plane direction was 5000-17000 S/m. In-plane conductivities were also examined by Williams *et al.* (2004) and found to be in the range of 5000-23000 S/m. They experimented with several types of PTLs including both carbon cloth and paper. PTLs from Toray Industries Inc. measured in-plane conductivities between 1.72-2.13 $\times 10^4$ S/m and a through-plane conductivity of 1750 S/m. The specification sheet on SGL Carbon's website (2008) indicates an in-plane conductivity 4-6 times that of the through-plane conductivity (333 S/m). Electronic conductivities measured by SGL Carbon were used in the model. Regarding the porosity, Barbir (2005) reported values between 0.8-0.9 but for an uncompressed PTL. Other sources, such as Wang *et al.* (2004) report porosities near 0.5. For this model it was assumed the porosity would be somewhere in between these two values and 0.65 was used.

Recently, PEMFC modelers have started to examine the consequences of implementing anisotropic conductivity assumptions in their models because anisotropy may have an important influence on the current-density distribution in the catalyst layer. Sun *et al.* (2005b) conducted a parametric study on a 2D steady-state cathode model, in which the conductivity in the in-plane direction was assumed to be ten times higher than the through-plane direction, which was 100 S/m. Both the magnitude and shape of the current-density distribution were affected by this change. In general, electron transport to areas under the channel was no longer limiting at low to mid-range current densities. The high conductivity in the in-plane direction allows for the improved transport of electrons to areas of the electrode that are under the gas channels. In one case, the area of maximum current density shifted from the channel and land boundary to the area solely under the channel.

Pharoah *et al.* (2006) used detailed simulations to examine the influence of several transport coefficients, such as mass diffusivity, electronic conductivity and hydraulic permeability, within the PTL of a PEMFC. Similar conclusions to those of Sun *et al.* (2005b) were made regarding the shift in the current density profile in the anisotropic case. The maximum current density was shown to shift from under the land to under the channel at two different cell voltages. Polarization curves were simulated for the isotropic and anisotropic cases, and Pharoah *et al.* (2006) concluded that the overall performance for both the anisotropic and isotropic case were very similar; however, the current density profiles were remarkably different. Thus, it is important that a polarization curve is not utilized as the sole tool for assessing PEMFC performance and endeavouring to improve it, because polarization curves do not provide sufficient information.

Zhou and Lui (2006) presented a 3-D model of a PEMFC, which they used to predict the effect of in-plane conductivities on the current density in the catalyst layer. They simulated five different cases wherein the electronic conductivity of the PTL was varied. Toray carbon paper was used as the base case, with 1250 S/m through-plane conductivity and 17200 S/m in-plane conductivity. To test the effect of in-plane conductivity they ran additional cases at 1500, 300, 100 S/m and infinite conductivity; while keeping the through-plane conductivity at 300 S/m. The polarization curves did not vary significantly, i.e., the simulations showed less than a 5% power loss from the base case. Zhou and Lui also examined the current density at several cell voltages to determine whether the in-plane conductivity had any effect on the current-density profiles across the land and channel. At a high cell voltage (0.8V), the maximum current was observed to be under the channel for all but one case. Oxygen diffusion was the clear limiting factor in this set of simulations run by Zhou and Lui, except for the case run at the lowest conductivity where the

maximum current was between the channel and land. The same cases were run at a lower cell voltage (0.5V) and the area of maximum current occurred between the land and channel for all but the perfect conductor. Intuitively, this is not the expected result. At higher current densities, oxygen diffusion becomes more of a limiting factor and the area of maximum current should remain under the channel. In the end, Zhou and Lui concluded that the in-plane and the through-plane conductivity do not significantly effect the current density distributions or the polarization curve, except in extreme cases. They suggested that the influence of anisotropic PTL conductivity can be ignored when designing PEMFCs. However, they did not consider PTL anisotropy effects simultaneously for electronic conductivity and mass diffusivity.

In Chapter 3 a steady-state 2 D cathode model is presented. This agglomerate model captures key transport and kinetic phenomena in the catalyst layer so that the model can provide useful predictions in regards to the reaction order of the ORR. It is important to understand the transport of electrons, protons and oxygen to the reaction sites and the kinetics of the ORR at these sites. The model does not include thermal or liquid water effects due to the complexity of two-phase flow.

Chapter 3

Cathode Model

3.1 Introduction

This chapter describes the two-dimensional (2D) steady-state cathode model developed in this thesis. The model considers the coupled transport and reaction phenomena in the catalyst layer. Electrochemical half-reactions occur at each electrode which involve both chemical (oxygen and water) and electrical (electrons and hydrogen protons) species. The transport phenomena associated with each species are important elements in PEMFC cathode simulations. These species are transported through the cathode, the PTL and catalyst layer domains, via separate phases and modes of transport. The following section provides a description of the material components that make up the cathode and the influence they have on the transport phenomena of the species that participate in this electrochemical reaction.

3.2 Model Description

3.2.1 Physical and Chemical Phenomena Considered

The key components and basic operations of a polymer electrolyte membrane fuel cell (PEMFC) have been discussed in Chapter 1. The present model is concerned with the PEMFC cathode wherein the reaction and transport in the cathode PTL and catalyst layer are modeled. The effect of bipolar plate geometry is considered since the pathway for electron transport is affected by the land area in contact with the PTL. To elaborate, it must be first realized that three distinct species participate in an electrochemical reactions – electrons, ions and chemical species. In the case of

the PEMFC cathode, the transport of the three types of species – electrons, protons, and chemical species (oxygen and water vapor) – is governed by the relevant driving force (potential gradient) and the effective transport properties of the media through which they are transported. The pathways taken by the species participating in the electrochemical reaction are further affected by the macro- and micro-scale features of the fuel cell sub-components. For example, the electron transport is affected by the rib or land size (macro-effect) of the flow field plate and by the microstructure of the carbon in the PTL.

A description of the key physical and chemical phenomena considered in the 2-D model developed is provided below. The basic 2-D geometry of the cathode is shown in Fig 3.1. The flow-field plate (bipolar plate) supplies oxygen and allows the transport of electrons; however, the transport of these species in the flow-field plate is not included in the model. Instead, the flow-field geometry effects are implemented via appropriate boundary conditions for the oxygen and electron transport equations. Oxygen is transported from the channels through the pores of the PTL to the catalyst layer. The electrons are transported from the land of the flow-field plate to the electron-conducting solid portion of the PTL to the catalyst layer. The protons for the electrochemical reaction are generated at the anode (not modeled) and arrive at the cathode catalyst layer through the polymer electrolyte (not modeled). The cathode electrochemical reaction produces water that is considered to exist only in vapor phase (or dissolved in the ionomer of the catalyst layer) and is transported from the catalyst layer through the pores of the PTL to the channels. The transport of the various species in the catalyst layer is coupled with the electrochemical reaction. The catalyst layer is considered to be composed of aggregates of spherical agglomerates of Pt/C and ionomer. The electrochemical reaction occurs at the two-phase boundaries (not triple-phase boundaries as is generally thought) where Pt and ionomer

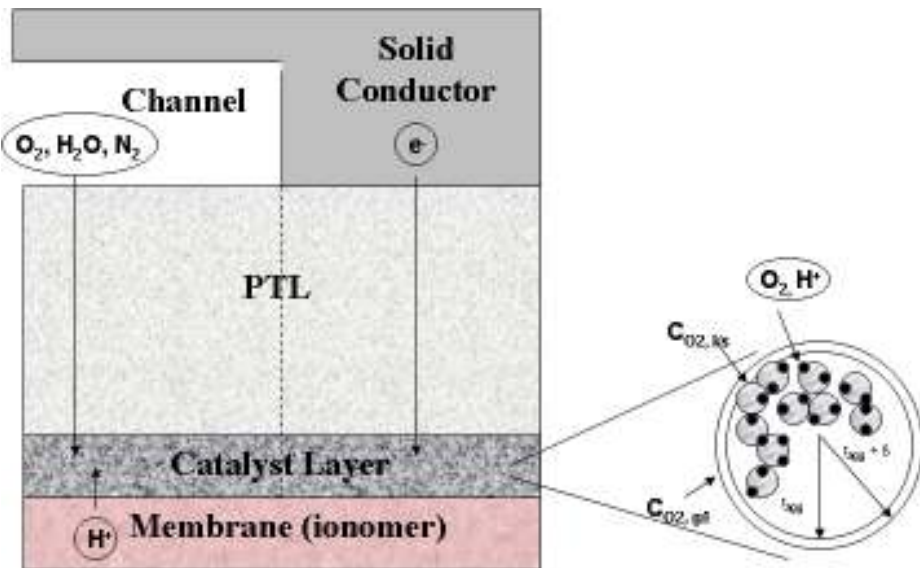


Figure 3.1: 2D-diagram of cathode domain. The solid flow-field plate conductor and membrane are not included in the model.

meet. Ionomer surrounding the catalyst particles facilitates the transport of protons and dissolved oxygen to the catalyst sites whereas the electrons are transported through the carbon phase. It is important to recognize that only those two-phase boundaries are active for electrochemical reactions. The carbon and ionomer at the two-phase boundary must be simultaneously connected to respective percolating networks so that electrons and protons can be transported to the boundary. Within the agglomerate, electrons are transported through the carbon support of the Pt/C catalyst, the protons are transported through the ionomer (polymer electrolyte) phase, and the oxygen is transported through the ionomer phase in a solvated state. Thus, oxygen arriving in the catalyst layer in a gaseous form is considered to dissolve into the ionomer phase prior to being transported to the active reaction sites.

Aside from the physical and chemical processes that occur in a PEMFC, there are also energy (or heat) transfer considerations such as thermal energy released in cathode half-reaction, which are not modeled in the current isothermal model. Note that condensation and evaporation associated with two-phase water transport also leads to heat effects. Resistive or ohmic heating results from the conduction of protons and electrons through all components of the PEMFC. Thus, considerable geometric complexity exists even at the single-cell level. Other effects such as flow distribution to various cells and heat transfer between cells become important in stack level models. A PEMFC stack is typically composed of 50 to 100 cells in series. Each cell in the stack is made up of several distinct components – bipolar plate, porous carbon based porous transport layer (PTL), catalyst layer and a polymer electrolyte membrane.

In a stack, bipolar plates connect the individual cells in series and provide a path for electrons to travel from the anode of one cell to the cathode of an adjacent cell. As well, each plate has channels that distribute the oxygen (or air) to the cathode and hydrogen to the anode. The anode and cathode both have a carbon layer (PTL) that transports the gaseous species and electrons needed in the half-reactions. Electrons are conducted through the carbon matrix and oxygen, nitrogen and gaseous water are transported through the pores via diffusion.

The electrochemical half reactions occur at the cathode and anode catalyst layer. Hydrogen gas enters the anode and dissociates into hydrogen ions (protons) and electrons at the catalyst sites in the anode catalyst layer. At the cathode, oxygen gas and the electrons from the adjacent cell's anode are transported to the catalyst layer where they react with the protons that have passed through the ionomer membrane. This membrane, which separates the cathode and anode, is composed of a polymeric material (often Nafion™) that possesses high ionic conductivity in the

presence of water, but offers low permeability to hydrogen and oxygen gases. The water is transported through the membrane through a combination of electroosmotic drag and diffusion.

3.2.2 Model Domain

As discussed above, the model domain considers the PTL and the catalyst layer of the cathode half-cell as shown in Fig. 3.2. The domain spans half the width of a flow-field-plate channel, and half the width of the flow-field-plate land that separates the channels. The PTL sub-domain is bounded by the land and channel at $z = z_{PTL}$ and the catalyst layer sub-domain at $z = z_{CL}$. The area under the channel covers the region between x_0 and x_{GC} and the area under the land between x_{GC} and x_L . The second sub-domain is the catalyst layer that is bounded by the PTL and the membrane at z_0 . The membrane, anode and bipolar plates are not included in this model.

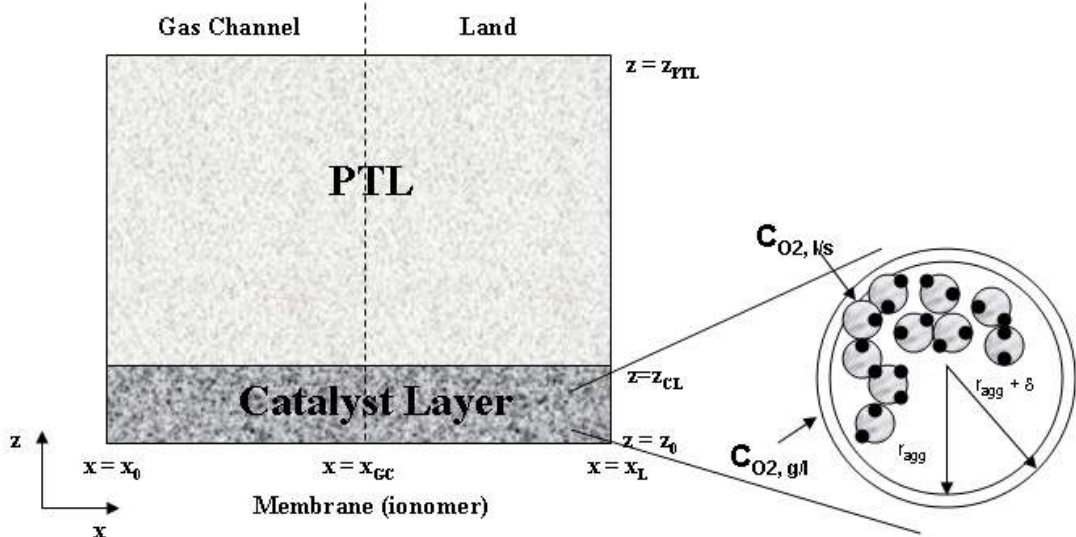


Figure 3.2: Domain of 2D cathode model. Agglomerate is shown with interstitial and surrounding ionomer film (white). Carbon particles (gray spheres) with platinum (black) on the surface are distributed inside the agglomerate. Note: figure is not to scale and the catalyst layer is thinner than it appears in the diagram.

3.2.3 Model Assumptions

The following assumptions were used in the PEMFC cathode model:

1. The PEMFC operates at steady-state.
2. There are no temperature gradients in the model (heat transfer effects are ignored). It is isothermal in both sub-domains.
3. Only gas-phase transport is considered, liquid water effects are ignored.
4. The catalyst layer is composed of aggregates of spherical agglomerates comprising Pt/C and ionomer.
5. Agglomerates are surrounded by a thin film of uniform thickness, which oxygen must dissolve into to access the catalyst reaction sites.
6. The PTL is anisotropic for both conductive and diffusive transport. The catalyst layer is isotropic.
7. Reaction kinetics are first-order with respect to the oxygen concentration. Note that half order reactions are considered in Chapter 4.
8. The land boundary has a potential of zero.
9. There is a constant ionic potential at the membrane boundary.
10. All oxygen transported into the catalyst layer is consumed.
11. The catalyst layer and PTL are considered homogeneous and detailed structure such as decreased porosity under the land due to compression is not considered.

3.2.4 Transport and Reaction Modeling

Electronic Transport

Electron transport occurs in both the carbon structure of the PTL and the carbon catalyst particles of the catalyst layer. The electron transport is described by Ohm's law relating the current density to the electronic phase potential gradient and the effective electronic conductivity of the carbon structures accounting of anisotropy of the PTL. As per the steady-state assumption, all electrons transported to the catalyst layer are assumed to participate in the reaction. In the PTL, since no reaction takes place, electrons are consumed nor created. The electron balances in each sub-domain are shown in the Table 3.1 and the corresponding source term for the balance within the catalyst layer is provided Table 3.2.

Ionic Transport

Ionic conduction occurs only in the catalyst layer (because there is no ionomer in the PTL) and is described by Ohm's Law. Accordingly, the protonic current density is the product of the protonic potential gradient and the effective ionic conductivity of the catalyst layer. Protons are consumed at the same rate as electrons in the ORR half-reaction. The sink term in the proton balance is negative, however, because protons and electrons have the opposite charge. Tables 3.1 and 3.2 list the proton balance and source term, respectively, for the catalyst layer.

Chemical Species Transport

Oxygen, nitrogen and water are three gaseous species that are transported through the porous structure of the cathode via diffusion. Diffusive transport is assumed to be governed by Fick's

Law. In Fick's Law, the molar flux of the chemical species is a product of the concentration gradient of transported species and the effective diffusion coefficient of the species in the gaseous mixture. The diffusion coefficients are modified to account for the tortuous path taken by the gaseous species through the porous media (PTL and catalyst layer) using a Bruggeman type correlation (discussed in detail in section 3.4.1) to yield effective diffusion coefficients. The divergence of the molar flux of each species in the PTL is zero since there are no sink or source terms considered in this sub-domain. All oxygen that enters the catalyst layer is assumed to be consumed. Nitrogen is not consumed and the source term for this material balance is zero. Water is produced at a molar rate twice that of oxygen consumption, according to the half-reaction stoichiometry. Also, water enters the catalyst layer from the ionomer membrane. Water assists in the transport of protons from the anode so that the rate of water transport through the membrane is proportional to the rate of protons consumed in the catalyst layer. An electroosmotic drag coefficient is defined to calculate the rate of water transport through the membrane. Mass balances for each of the gaseous species and the associated source terms are shown in Tables 3.1 and 3.2.

Oxygen Reduction Reaction (ORR)

As discussed above, the cathode electrochemical reaction, i.e., the oxygen reduction reaction (ORR) occurs at the active *two-phase* boundary where the Pt/C phase meets with ionomer phase. The electrochemical reaction rate is described using Butler-Volmer kinetics (Madhusudana, *et al.*, 2007). Thus, as dictated by the electrochemical kinetics, the local reaction rate is a function of the phase potential of the three species, i.e., the chemical potential, and the ionic and electronic phase potentials. In more familiar terms, the reaction rate is a function of the oxygen concentration and the overpotential (the deviation of the difference in the electronic and ionic

phase potentials from the difference of the phase potentials at equilibrium conditions). The phase potentials of each species vary in the catalyst layer as required by the relevant governing conductive-diffusive transport mechanisms, and, thereby, the reaction rate varies throughout the catalyst layer. Referring to Fig 3.2, it can be readily understood that the concentration of oxygen varies in the z-direction because it is consumed as it diffuses through the catalyst layer and in the x-direction, because the diffusion path for the oxygen through the PTL to the portion of the catalyst layer under the land is longer than the path to the catalyst layer directly below the gas channel.

In the model, a further complexity is added by noting that the catalyst layer is composed of spherical agglomerates. The building blocks of an agglomerate, shown in Fig 3.2, are platinum-dispersed carbon particles and polymer electrolyte. The aggregates of Pt/C particles are held together by the polymer electrolyte. The model also considers that each agglomerate particle is surrounded by a thin, ionomer membrane with uniform thickness, δ . Oxygen is transported in gaseous state through the pores between the spherical agglomerate particles. It dissolves in the ionomer and then diffuses through the ionomer (surrounding and within the agglomerate) to the carbon particles where it reacts on the surface of the platinum. Within the agglomerate, a radial concentration gradient exists because oxygen is consumed as it diffuses through the agglomerate toward the centre. Thus, oxygen concentration varies in three spatial dimensions (x, z and r). However, by invoking a pseudo-homogeneous assumption, the equations are solved in x- and z-direction only and the radial direction variability is handled through *an effectiveness factor* approach that is described in many textbooks on reaction engineering (e.g., Fogler, 2005). The effectiveness factor (E_r) allows calculation of the reaction rate in a spherical particle, knowing the surface reaction concentration.

The reaction rates (source and sink) terms are listed in Table 3.2. Detailed derivation of the form of equation has been reported by Sun *et al.* (2005a) and is not presented here. The key parameters of the source terms are the effectiveness factor (E_r), the thickness of ionomer film surrounding an agglomerate (δ), and the electrochemical reaction rate constant (k_c).

ORR Kinetics and Effectiveness Factor

For the results presented in this Chapter, first-order kinetics reported by Parthasarathy *et al.* (1992a) was employed. Specifically, the reaction rate is assumed to be proportional to the concentration of oxygen (raised to the power of one) in the catalyst layer. Where an electrochemical reaction rate constant, k_c , is the proportionality constant. The electrochemical reaction rate constant, k_c , is determined using the Butler-Volmer equation and is a function of the temperature and overpotential. In addition, several electrochemical kinetic parameters – exchange current density and charge-transfer coefficients are required to compute k_c (See Appendix B for the equation used to calculate k_c).

The net rate of oxygen consumption in an agglomerate is the product of E_r , k_c and $C_{O_2,I/s}$ the oxygen concentration at the inner surface of the ionomer film (see Fig. 3.2) surrounding each agglomerate particle. The effectiveness factor is calculated based on a parameter known as the Thiele modulus, Φ_L (Fogler, 2006). The Thiele Modulus is a dimensionless group that includes the radius of the agglomerate, the electrochemical reaction rate constant (k_c) and the effective diffusion coefficient of oxygen in the ionomer.

3.3 Model Equations and Boundary Conditions

The model equations that are solved and the associated boundary conditions are presented in this section, as are numerical values for model parameters and correlations used for obtaining effective transport properties.

3.3.1 Model Equations

Table 3.1: Summary of transport equations for chemical, electronic and ionic species.

	Species	Transport Equations
Porous Transport Layer (PTL)	Oxygen	$\nabla \cdot j_{O2,P} = \nabla \cdot (-D_{O2m,P}^{eff} \nabla c_{O2}) = 0$
	Water	$\nabla \cdot j_{H2O,P} = \nabla \cdot (-D_{H2Om,P}^{eff} \nabla c_{H2O}) = 0$
	Nitrogen	$\nabla \cdot j_{N2,P} = \nabla \cdot (-D_{N2m,P}^{eff} \nabla c_{N2}) = 0$
	Electrons	$\nabla \cdot i_{e,P} = -\nabla \cdot (k_{e,P}^{eff} \nabla \phi_{e,local,P}) = 0$
Catalyst Layer	Oxygen	$\nabla \cdot j_{O2,C} = \nabla \cdot (-D_{O2m,C}^{eff} \nabla c_{O2}) = S_{O2,C}$
	Water	$\nabla \cdot j_{H2O,C} = \nabla \cdot (-D_{H2Om,C}^{eff} \nabla c_{H2O}) = S_{H2O,C}$
	Nitrogen	$\nabla \cdot j_{N2,C} = \nabla \cdot (-D_{N2m,C}^{eff} \nabla c_{N2}) = 0$
	Electrons	$\nabla \cdot i_{e,C} = -\nabla \cdot (k_{e,C}^{eff} \nabla \phi_{e,local,C}) = S_{e,C}$
	Protons	$\nabla \cdot i_{p,C} = -\nabla \cdot (k_{p,C}^{eff} \nabla \phi_{p,local,C}) = S_{p,C}$

Table 3.2: Summary of source terms, boundary for each domain. Boundary conditions for the gaseous species are given in mass fractions.

	Species	Source/sink Term	Boundary Conditions
Porous Transport Layer (PTL)	Oxygen	-	Land: No flux Channel: 0.209 Remaining Boundaries: No flux
	Water	-	Land: No flux Channel: 0.103 Remaining Boundaries: No flux
	Nitrogen	-	Land: No flux Channel: 0.688 Remaining Boundaries: No flux
	Electrons	-	Land: 0 V Channel: No flux Remaining Boundaries: No flux
Catalyst Layer	Oxygen	$\frac{M \times w_{O_2} \times P}{H} \left(\frac{1}{E_r k_c (1 - \varepsilon_{CAT})} + \frac{(r_{agg} + \delta) \delta}{Da_{agg} r_{agg}} \right)^{-1}$	Membrane: No flux Remaining Boundaries: No flux
	Water	$2 \times (1 + 2\alpha) \times \left(\frac{M_{H_2O}}{M_{O_2}} \right) \times \frac{M \times w_{O_2} \times P}{H} \left(\frac{1}{E_r k_c (1 - \varepsilon_{CAT})} + \frac{(r_{agg} + \delta) \delta}{Da_{agg} r_{agg}} \right)^{-1}$	Membrane: No flux Remaining Boundaries: No flux
	Nitrogen	-	Membrane: No flux Remaining Boundaries: No flux
	Electrons	$4F \frac{M \times w_{O_2} \times P}{M_{O_2} H} \left(\frac{1}{E_r k_c (1 - \varepsilon_{CAT})} + \frac{(r_{agg} + \delta) \delta}{Da_{agg} r_{agg}} \right)^{-1}$	Membrane: No flux Remaining Boundaries: No flux
	Protons	$4F \frac{M \times w_{O_2} \times P}{M_{O_2} H} \left(\frac{1}{E_r k_c (1 - \varepsilon_{CAT})} + \frac{(r_{agg} + \delta) \delta}{Da_{agg} r_{agg}} \right)^{-1}$	Membrane: ϕ_p Remaining Boundaries: No flux

3.3.2 Boundary Conditions

Appropriate boundary conditions were applied to each sub-domain to solve the relevant transport equations for each species. The boundary conditions used in this model are summarized in Table 3.1. The boundaries at x_0 and x_L are considered symmetrical for both sub-domains. It is assumed that identical domains would border the current domain if the model were expanded in the x-direction. As a result, the flux of each of the chemical species as well the electronic and ionic species is set to zero across the boundaries in the x direction.

Electronic Species

A reference potential of 0 V is specified arbitrarily at the land/PTL boundary, z_{PTL} . Other boundaries in the cathode domain were set using zero-flux conditions because electrons are not transported through the membrane or into the channel.

Ionic Species

Proton transport is assumed to be negligible in the PTL subdomain, therefore the flux at the z_{CL} boundary is zero. The ionic-phase potential, ϕ_p , at the membrane boundary, z_0 , is an input variable that is assigned a value before running the simulation. The difference between the ionic potential at the membrane boundary and the electron potential at the land boundary is referred to as the nominal cathode overpotential (NCO). It includes all the losses in the cathode between the boundaries (i.e., the activation, ohmic and concentration overpotentials).

Chemical Species

As shown in Table 2.1, the oxygen, nitrogen and water mass fractions at the PTL/channel boundary were set at 0.209, 0.688, and 0.103, respectively, (or 0.177, 0.667, 0.134 molar fractions) for the simulations in this chapter, based on an assumed standard composition for dry air of 21 mole % oxygen and 79 mole % nitrogen and 50% relative humidity at a temperature of 80 °C. The remaining boundaries, the land (z_{PTL}) and the membrane (z_0), do not permit the flux of gaseous species, and the flux boundary condition was set to zero.

3.3.3 Model Parameters

Operating conditions used in the model are provided in Table 3.3, and model parameters are listed in Table 3.4.

Table 3.3: *Operating conditions considered for the model. Oxygen and water concentrations were varied in the study presented in section 4.9.*

Temperature	353.15	K-
Pressure	1.5	atm
Concentration at the channel boundary		
Oxygen	9.18	mol/m ³
Nitrogen	34.53	mol/m ³
Water	6.97	mol/m ³
RH	50	%

Table 3.4: Model Parameters

CL porosity	0.1	-	
PTL porosity	0.65	-	Barbir (2005), Wang <i>et al.</i> (2004)
Ionomer film thickness	80	nm	Kulikovsky <i>et al.</i> , 2000
Agglomerate radius	1.0	μm	Jaouen <i>et al.</i> , 2002, Siegel <i>et al.</i> , 2003
Fraction of ionomer in catalyst layer	0.5	-	Kulikovsky <i>et al.</i> , 2000
Reference exchange current density	3.85e-4	A/m ²	Parthasarathy <i>et al.</i> , 1992a, 1992b
Reference oxygen concentration	0.851	mol/m ³	Parthasarathy <i>et al.</i> , 1992a, 1992b
Cathodic transfer coefficient	1.0	-	Parthasarathy <i>et al.</i> , 1992a, 1992b
Henry's constant	0.3125	atm m ³ /mol	Parthasarathy <i>et al.</i> , 1992a
Diffusivity of oxygen in nafion	8.786e-10	m ² /s	Parthasarathy <i>et al.</i> , 1992a, 1992b
Thickness of CL	15	μm	Broka <i>et al.</i> , 1997.
Conductivity in through-plane of PTL	1667	S/m	SGL Carbon, 2008
Conductivity in in-plane of PTL	333	S/m	SGL Carbon, 2008
Effective platinum surface ratio	0.75	-	Cheng <i>et al.</i> , 1999

3.3.3.1 Effective Transport Properties

Effective Diffusion Coefficients

Diffusion coefficients for species in gas mixtures can be calculated from binary diffusion coefficients of the various species (Bird *et al.* 1960) using the following correlation (Wilke, 1950):

$$D_{im} = \left(1 - x_i\right) \left(\sum_{j=1; j \neq i}^n \frac{x_j}{D_{ij}} \right) \quad (3)$$

In the PTL, the effective diffusivity of each gaseous species is influenced by the PTL structure, which is highly anisotropic. Hamilton (2005) performed direct numerical simulations of conductive transport through both the solid and pore regions of a computer-generated reconstruction of carbon paper. The simulation results yielded effective electronic conductivity and gas-phase diffusivity for both in-plane and through-plane directions. The randomly laid fibres of the carbon paper were fit to the following correlations:

$$\begin{aligned} \text{In-plane: } D_{im,p}^{eff} &= D_{im} \varepsilon_p^{1.673} \\ \text{Through-plane: } D_{im,p}^{eff} &= D_{im} \varepsilon_p^{1.97} \end{aligned} \quad (4)$$

where ε_p is the porosity of the PTL. Since the catalyst layer is assumed to be isotropic, a simple Bruggemann correlation is used in the model to obtain effective diffusion coefficients within gas pores of the catalyst layer.

$$D_{im,c}^{eff} = D_{im} \varepsilon_{CAT}^{1.5} \quad (5)$$

where ε_{CAT} is the porosity of the catalyst layer, assuming that the aggregates are dense spheres.

Effective Ionic Conductivity

The ionic conductivity of ionomer membranes has been studied and found to be a function of the temperature and water content of the membrane by Springer et al. (1991). They developed the following relationship to determine the conductivity:

$$k_p = 100[0.005139\lambda - 0.00326\left[1268\left(\frac{1}{303} - \frac{1}{T + 273.15}\right)\right]] \quad (6)$$

where, λ is the water content of the membrane. Assuming no liquid water in the catalyst layer, West and Fuller (1996) found that the water content could be calculated knowing the relative humidity (RH).

$$\lambda = 0.3 + 10.8RH - 16RH^2 + 14.1RH^3 \quad (7)$$

In the current model, the effective ionic conductivity is calculated using the Bruggemann relationship (Sun *et al.*, 2005a):

$$k_p^{eff} = k_p [(1 - \varepsilon_{CAT}) \varepsilon_{agg}]^{1.5} \quad (8)$$

where ε_{agg} is the fraction of ionomer within each aggregate.

Effective Electronic Conductivity

The electronic conductivity of carbon papers has been reported by several product suppliers. Few manufacturers provide in-plane conductivity information, but the specification sheet on SGL Carbon's website (2008) indicated that the in-plane conductivity is 4-6 times that of the through-plane conductivity. Therefore, the through and in-plane conductivity were set at 333 S/m and 1667 S/m, respectively, in the model. A Bruggemann relationship was used to calculate the effective electronic conductivity of the catalyst layer by considering the phase fraction of platinum-covered carbon particles:

$$k_e^{eff} = 333 [(1 - \varepsilon_{CAT})(1 - \varepsilon_{agg})]^{1.5} \quad (9)$$

3.3.3.2 Kinetic and Reaction Parameters

Exchange Current Density

The exchange current density is an important kinetic parameter, which is specific to a given catalyst/ionomer system and also depends on the operating conditions such as the temperature and pressure. The following correlations were developed by Sun *et al.* (2005a), based on experimental data from Parthasarathy (1991a, 1991b).

$$\log(i_0^{ref}) = \log(P_{O_2}) - 7.89 \text{ at T=323K}$$

$$i_{0,2}^{ref} = i_{0,1}^{ref} \exp\left(\frac{-\Delta E_{exc}}{R}\left(\frac{1}{T_2} - \frac{1}{T_1}\right)\right) \quad (10)$$

where, ΔE_{exc} is the activation energy of the ORR(76.5 kJ/mol as determined by Parthasarathy (1991b)). The partial pressure of oxygen and temperature are 0.265 atm and 80°C, respectively, which are the operating conditions at the channel boundary.

To calculate the current densities in terms of the unit area or volume of the catalyst layer a property relating the surface area of platinum to the catalyst layer dimensions is needed. The total Pt surface area per unit volume of catalyst layer, a_{pt} , is a function of the catalyst loading, m_{Pt} , the thickness of the layer, t_{cl} and the surface area per unit mass of platinum particles, S_{ac}

$$a_{pt} = \frac{m_{Pt} S_{ac}}{t_{cl}} \quad (11)$$

Since the electrochemical half reaction requires two phases, the platinum and ionomer, to be in contact, only a fraction of the platinum surface area is available for the reaction and an effective property, a_{Pt}^{eff} is used. The ratio of the platinum area in contact with the ionomer to the total platinum surface area is defined as f_{Pt} .

$$a_{Pt}^{eff} = f_{Pt} a_{pt} \quad (12)$$

Charge-Transfer Coefficient

The charge-transfer coefficient, α_c can be obtained from a Tafel plot, where overpotential is plotted against the logarithm of the current density. A value of $\alpha_c=1.0$ was used in the model, for all values of NCO, based on experimental results from Parathasarthy *et al.* (1991a).

Thiele Modulus and Effectiveness Factor

In an electrochemical reaction governed by first-order reaction kinetics, the Thiele Modulus is defined as:

$$\Phi_L = \frac{r_{agg}}{3} \sqrt{\frac{k_c}{D^{eff}}} \quad (13)$$

Thiele (1939) arrived at this result by completing a mass balance on a spherical particle (without a surrounding polymeric film).

The effectiveness factor as a function of the Thiele Modulus for a first-order reaction is:

$$E_r = \frac{1}{\Phi_L} \left(\frac{1}{\tanh(3\Phi_L)} - \frac{1}{3\Phi_L} \right) \quad (14)$$

where E_r is a ratio of the actual overall reaction rate for the particle to the reaction rate that would be obtained if the reactant concentration within entire particle were the same as the surface concentration. A low E_r , or high Φ_L , can result from either slow diffusion within the particle or from fast reaction kinetics, so that the reactant (oxygen) cannot penetrate easily into the particle before it is consumed appreciably.

3.4 Solution Method

The set of partial differential equations described in Table 3.1 was solved using the finite-element-based Multiphysics Modeling software COMSOLTM (see Appendix B for summary of equations used in the model). The finite element method (FEM) is a numerical technique that can be used to approximate the solution of a set of PDEs. The domain is discretized into a fine grid

of triangles or tetrahedra, which allows this technique to handle complex geometries. Polynomial basis functions (also called trial functions) at nodal values of the dependent variable are then used to represent the solution for each element. Since the basis functions are easily differentiated, the original PDEs are converted into algebraic functions of the basis function coefficients. The FEM solver determines appropriate values of the coefficients (and hence an approximate solution) to minimize a norm of the residuals for the solution vector.

An iterative, stationary, solver was used to solve this steady-state model. A relative tolerance of $1.0e^{-6}$ was set as the criterion for convergence for the sum of the absolute values of the scaled residuals. All of the settings used to solve the PDEs using COMSOLTM are provided in Appendix A. For each iteration, COMSOLTM estimates the errors and the solver terminates when the norm of the error is less than the chosen tolerance. The system of equations was solved for a number of different overpotentials. In each simulation case of interest, the ionic potential at the membrane boundary z_0 , (i.e. the NCO) was varied using a parametric version of the solver. The potential was incremented by 0.05 V each time to obtain sufficient simulation points to construct a predicted polarization curve. The simulations were performed on a desktop computer with a Pentium 4 2.8 GHz processor, 512 MB of RAM and a Windows XP operating system.

3.4.1 Mesh Matrix Used for Numerical Solution

The domain in Fig. 3.2 was divided into a triangular mesh, as shown in Fig. 3.3. There are 5912 elements in Fig. 3.3 a). The mesh was refined manually near the boundaries and the catalyst layer where larger gradients in the solution were observed. The elements in the catalyst layer subdomain were limited to a maximum size of $5.0 \bullet 10^{-6}$ m, the PTL sub-domain $2.5 \bullet 10^{-5}$ m and

the boundaries $1.0 \cdot 10^{-5}$ m. As well, the point where the land and channel boundaries meet was refined and specified using a $3.0 \cdot 10^{-6}$ m maximum size. A mesh study was completed, where a finer mesh with ~ 14000 mesh elements (Fig. 3.3 b) and an adaptive mesh with ~ 11000 mesh elements (Fig. 3.3 c) were used to obtain additional results so that a comparison could be made between the numerical results obtained using the various meshes. Additional meshes (a non-adaptive mesh with ~ 16000 elements and an adaptive mesh with ~ 8000 mesh elements) were also used in the grid study but are not shown in Fig. 3.3.

3.5 Results and Discussion

A polarization curve and current density plots at three different NCOs are shown in Figs. 3.4 and 3.5 below. It is useful to recall that NCO (nominal cathode overpotential) is defined as the difference between the ionic potential at the membrane boundary and the electronic potential at the land boundary. Thus, NCO encompasses the ohmic losses in the PTL and catalyst layer, as well as the activation losses. The NCO is used to determine the cell potential in the polarization curves, as it is the deviation from the theoretical reversible potential of the cathode, (1.15 V for the cathode half-reaction at the given operating conditions). For example, a NCO of 0.30 V corresponds to a cell potential of 0.85 V. The polarization curve was created by varying the NCO and obtaining corresponding predicted current densities. The current density plots (Fig. 3.5) illustrate how the maximum current density changes based on the cell voltage. At low current densities, electron transport resistance is the dominant resistance among the transport resistances of the three reacting species (electrons, protons and oxygen) and the maximum current density is under the land. The maximum shifts to under the channel as the current density is raised, where oxygen diffusion becomes limiting.

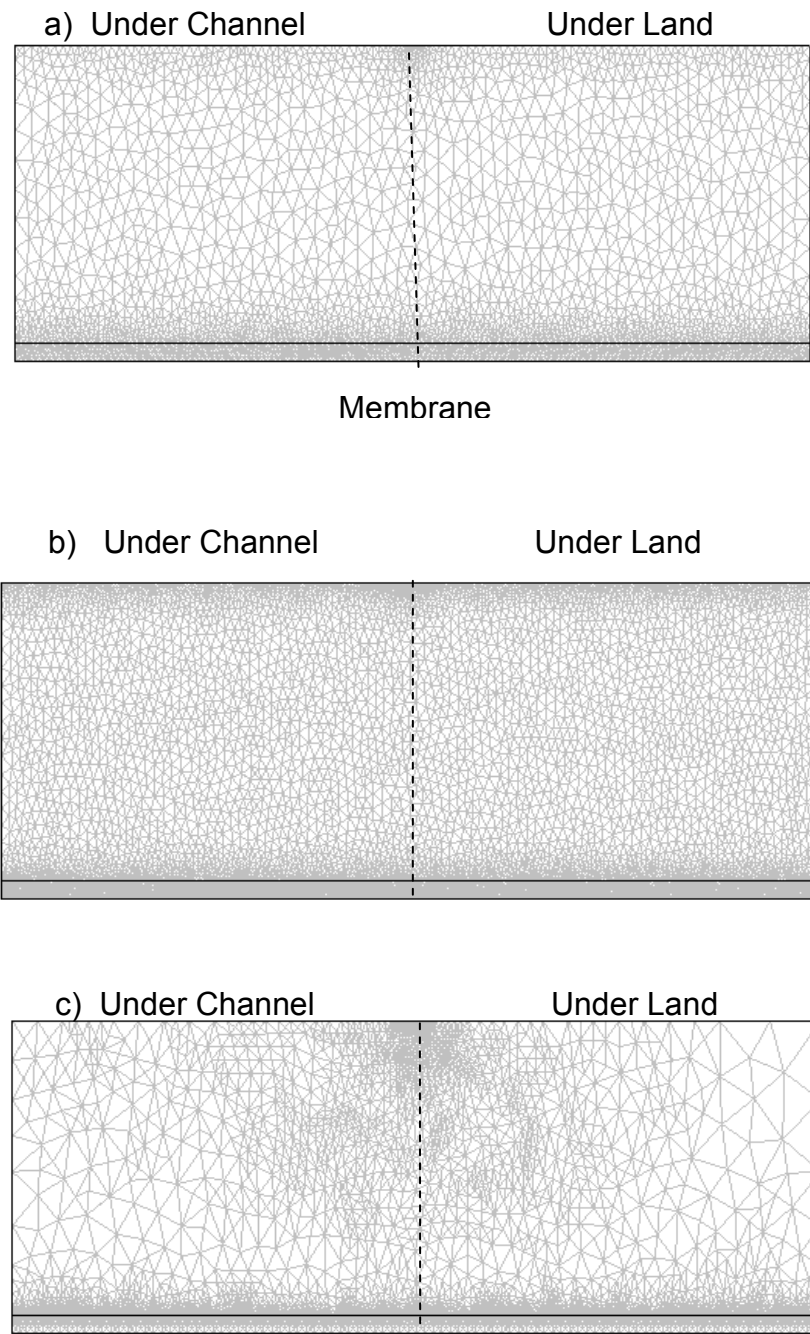


Figure 3.3: Mesh geometry of a) Coarse Mesh b) Fine Mesh c) Adaptive Mesh used in the base case model. This adaptive mesh was generated by COMSOL™ for simulations conducted using an overpotential of 0.3 V at the membrane/catalyst layer interface. Slightly different meshes were generated by COMSOL™ when higher overpotentials were simulated.

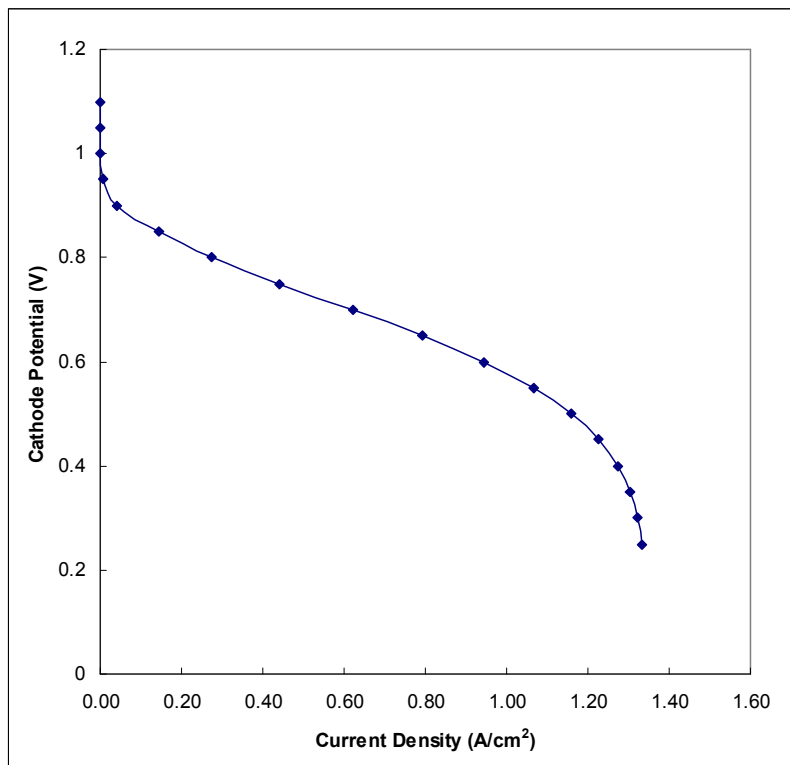


Figure 3.4: Predicted polarization curve of the 2D steady-state cathode model base case. The coarse mesh in Fig. 3.3 a) is used in this simulation.

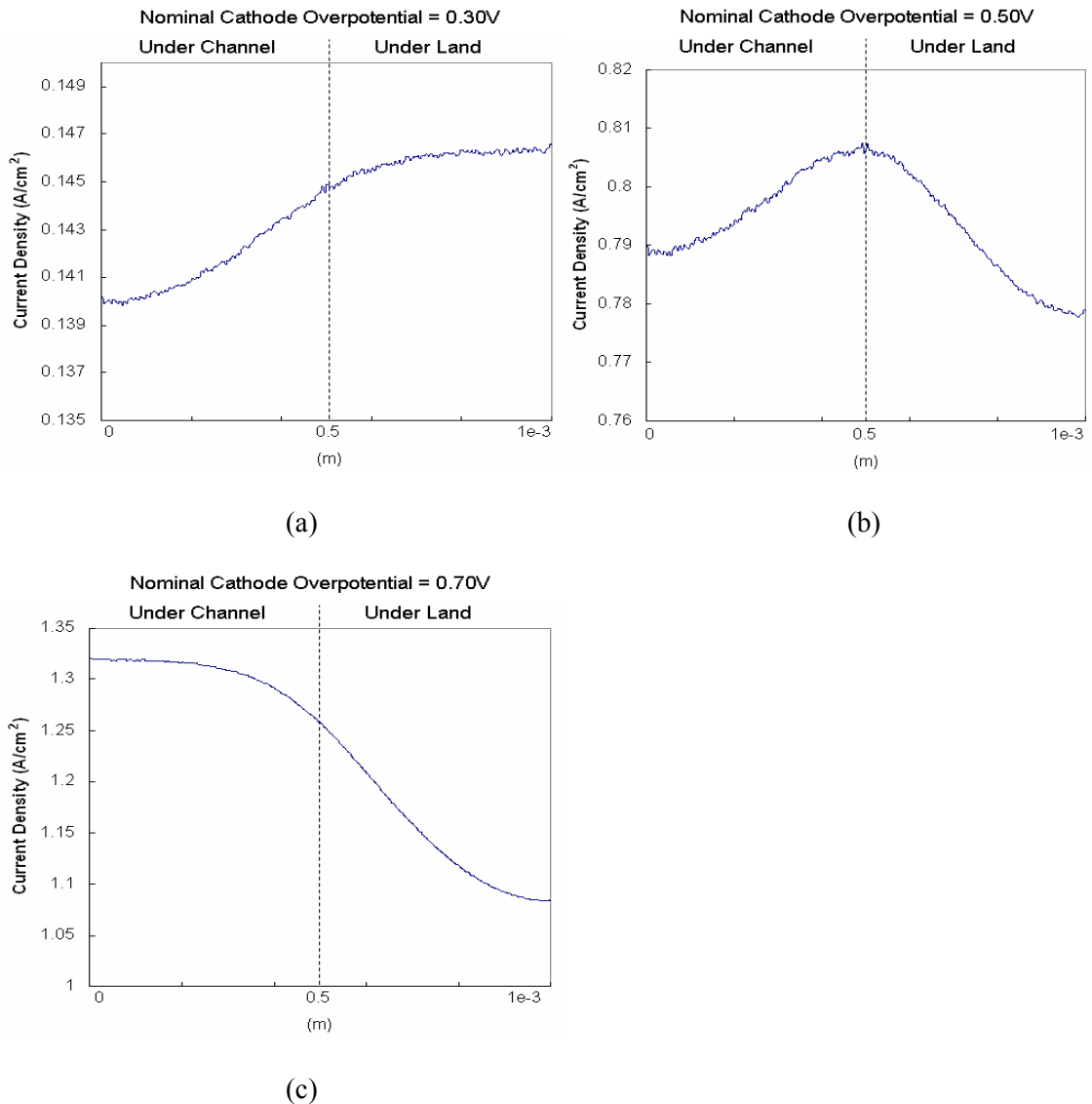


Figure 3.5: The current density distribution (A/cm^2) between the catalyst layer and membrane at a NCO of a) $0.3V$ b) $0.5V$ c) $0.65V$. The coarse mesh in Fig. 3.3 a) is used in this simulation.

3.5.1 Additional Considerations

Several shortcomings in the model were discussed in Chapter 2. Improvements designed to address these issues are presented in the current section. These improvements include – use of single kinetic parameter for whole range of polarization (rather than using two Tafel slopes), accounting for anisotropic electronic conductivity and gas diffusivity, and inclusion of concentration polarization. To elaborate, new values of the kinetic parameters, i_0 and α_c , are incorporated in the model. The isotropic conductivities and diffusivities of the PTL in Sun's model are replaced by more realistic anisotropic values. Finally, the local activation overpotential required to calculate the kinetic rate constant is adjusted to account for the concentration polarization resistances. Simulations were conducted to examine the influence of these improvements on the model predictions, and a polarization curve and current density plot (0.5 V) summarizing the influence of each of these changes is presented in Figs 3.6 and 3.7.

Effect of employing single kinetic Parameter for full polarization range

In the base case (using Sun's assumptions), α_c and i_0 were set at 1.0 and $3.85e^{-4}$ A/cm² respectively, below a NCO of 0.35 V and at 0.617 and 0.015 A/cm² above 0.35 V, to account for the double Tafel slope. The values of the parameters have been adjusted in this thesis so that α_c and i_0 , are constant at 1.0 and $3.85e^{-4}$ A/cm². As shown in Fig 3.6 the polarization curves are identical below a NCO of 0.30 V (i.e. at and above a cathode cell potential of 0.85 V) because the kinetic parameters are the same in both cases. However, above 0.35 V, the predicted cell performance is higher using the new constant parameters due to lower activation losses.

The cathodic transfer coefficient, α_c , has a larger influence on cell performance than the exchange current density. Although the new simulation results use a lower exchange current density at high voltages than Sun's model (which should impede fuel cell performance), it is shown in Fig. 3.6

that the polarization curve is shifted to the right due to the higher cathodic transfer coefficient, α_c . There is little change in the shapes of the current density curve (Fig. 3.7), compared to the base case. The adjustment to the kinetic parameters did not influence the location of maximum and minimum reaction rate, so the qualitative conclusions are still valid.

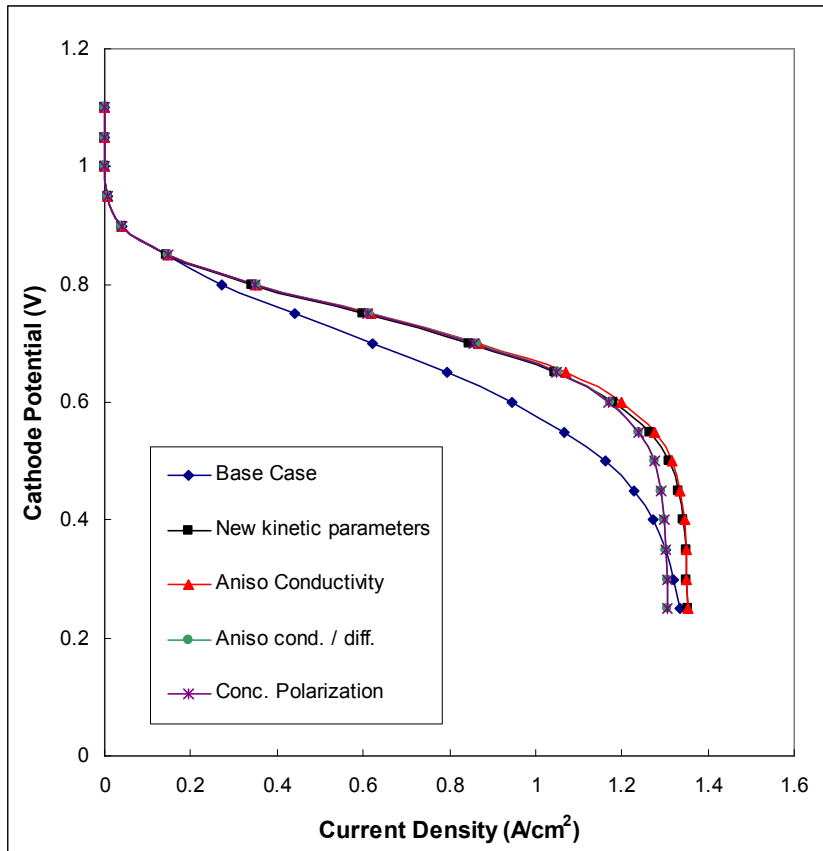


Figure 3.6: Predicted polarization curves comparing each additional change made to the original model. Updated kinetic parameters are used for i_0 and α_c . Anisotropic conductivity and diffusivity parameters are added to the PTL. As well, the concentration polarization is considered in the calculation of the reaction rate constant (note the curve is nearly coincidental with the aniso cond./diff. curve). Each subsequent change includes the previous modifications. The finest adaptive mesh settings (see Fig. 3.3 c) were used in these simulations.

Effect of Considering Anisotropic Conductivity

Two cases were considered, one where the isotropic conductivity is 333 S/m and another where the conductivity is 333 S/m in the through-plane direction and five times this value in the in-plane direction. At low current densities, there is virtually no difference between the current densities for the base case and the simulations with anisotropic conductivity. However, at increasing current densities, the anisotropic case results in higher current than the isotropic case, for the same cathode potential. This can be readily explained in terms of lower ohmic losses for the anisotropic case because the in-plane conductivity is five times higher than the isotropic and through-plane conductivity resulting in facile electron transport in the x-direction (in-plane). The difference in the polarization curves is minor, but larger changes are seen in current density plot in Fig. 3.7.

Fig. 3.7 illustrates the change in position of maximum current density, using an NCO of 0.5 V. For the isotropic cases (the base case and the isotropic simulation with new kinetic parameters), the maximum current density is between the land and channel, while for the anisotropic case the maximum is clearly under the channel. Electron transport limitations play an important role at average overpotentials near 0.50 V for an isotropic PTL; however, this is not the case for an anisotropic PTL. Oxygen diffusion is the dominant limiting transport mechanism in the catalyst layer in this case.

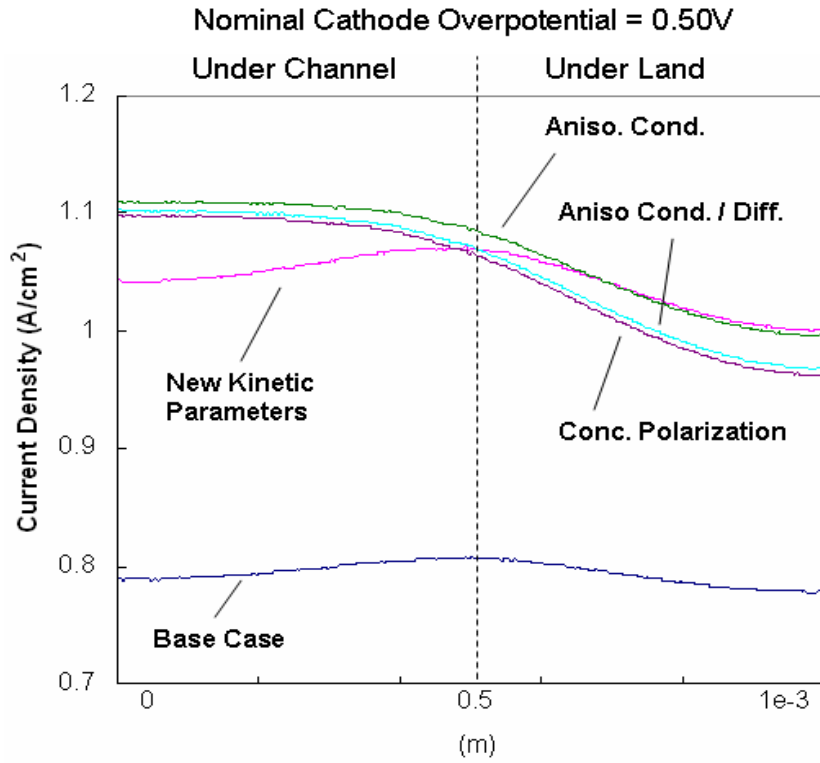


Figure 3.7: Current density plot at an NCO of 0.5 V. Curves are presented comparing each additional change made to the original model. Updated kinetic parameters are used for i_0 and a_c . Anisotropic conductivity and diffusivity parameters are added to the PTL. As well, the concentration polarization is considered in the calculation of the reaction rate constant. Each subsequent change includes the previous modifications. The finest adaptive mesh settings (see Fig. 3.3c) were used in these simulations.

Effect of Considering Anisotropic Diffusivity

As expected, the polarization curves start to diverge (between aniso cond. and aniso cond/diff) at high current densities where mass transport losses are important. The anisotropic case has a slightly lower current density than the isotropic case at the same cell potential due to the smaller diffusion coefficients in the in-plane and through-plane directions. The anisotropic case also reaches its limiting current density before the isotropic case because of the difference in the diffusion coefficients. The current density plot shows that the anisotropic diffusion coefficients

have little qualitative influence on the curves as opposed to the large effect that the anisotropic conductivities.

Effect of Including Concentration Polarization

The actual cell voltage, V_c , of a PEMFC is always lower than the theoretical maximum voltage, E_{rev} , due to losses in the cell. There are three types of resistances that contribute to the majority of the total loss in a PEMFC: activation, ohmic and mass transfer resistances.

$$V_c = E_{rev} - \eta_{act} - \eta_{ohm} - \eta_{conc} = E_{rev} - NCO \quad (15)$$

Activation losses, η_{act} , are associated with the kinetics of the reaction. The transfer of electrons to the surface of the catalyst and the activation energy required to drive the reaction both cause a loss in cell voltage. The transport of electrons and ions through the electrode (PTL and catalyst layer) is hindered by ohmic resistances, determined by the conductivity of the media, leading to the total ohmic loss in the cathode, η_{ohm} . Mass transport losses in the cathode, η_{conc} , are caused by the oxygen concentration gradient within the catalyst particles, which arises due to fast oxygen consumption compared with the rate of oxygen mass transport. The nominal cathode overpotential, NCO , is the sum of the losses in the cathode.

The reaction rate constant, k_c is a function of the local activation overpotential, η_{local} , which is the difference between the ionic and electronic potentials at a particular location in the catalyst layer. Sun *et al.* (2005a) determined η_{local} using,

$$\eta_{local} = NCO - \eta_{ohm} = \phi_{p,0} - \phi_{e,0} - \eta_{ohm} \quad (16)$$

where, $\phi_{p,0}$ is the ionic potential at the membrane/catalyst-layer boundary and $\phi_{e,0}$ is the electronic potential at the PTL/land boundary. Sun *et al.* did not include the mass-transport loss, η_{conc} , which should be subtracted from the right-hand side of Eq. (16) to give:

$$\eta_{local} = \phi_{p,0} - \phi_{e,0} - \eta_{ohm} - \eta_{conc} = \phi_{p,local} - \phi_{e,local} - \eta_{conc} \quad (17)$$

In this thesis, the concentration overpotential, η_{conc} , is accounted for using Eq. (17).

In Fig. 3.6 and 3.7 there is no discernable shift in the polarization curve when the concentration overpotential correction is applied, because the value of η_{conc} is relatively small compared to the activation overpotential (roughly two orders of magnitude lower). Even at high current densities, where mass transport is limiting and the concentration overpotential is at its highest, the polarization curves are nearly coincident. The reaction rate constant, k_c , at a medium NCO of 0.5 V is $2.69\text{e}^5 \text{ s}^{-1}$ before the correction and $2.53\text{e}^5 \text{ s}^{-1}$ after it. The current density is slightly lower when the correction to the local activation overpotential is made.

3.5.2 Grid Study

In FEM, a solution is computed by discretizing the domain into elements. The elements are referred to as mesh and in 2D domains they can be either rectangular or triangular. COMSOL™ uses a triangular mesh. The density of the elements in the domain can have an affect on both the accuracy of the solution and the computation time of the model. Two approaches were examined to create a mesh in COMSOL™, i.e., manually and using COMSOL's adaptive mesh method. The first case used a mesh divided into ~6000 elements (see Table 3.5 and Figure 3.3a) over the model domain, including both the PTL and catalyst layer sub-domains. Finer meshes were applied to the catalyst layer, the PTL region near the catalyst layer, and the land and channel

boundaries where gradients were largest. As well, the PTL region around the area where the land and channel meet was given a denser mesh. Two additional cases were simulated with finer meshes and were used to compare the predicted results from meshes with different densities to confirm the accuracy of the numerical solution. These new meshes had ~14,000 and ~16,000 elements (see Table 3.5). Simulations were run using the different meshes for NCOs of 0.3, 0.5 and 0.7 V. The computation time of the base case simulation was 290 seconds, and the simulation with the denser meshes had computation times of ~1900 seconds and ~3000 seconds. The resulting current density plots are shown in Fig. 3.8. At low overpotentials (0.30 V) there is a small difference in the current densities, about 0.13% between the coarsest and the densest mesh. At NCOs of 0.5 and 0.7 V there is little or no difference between the current density plots of each mesh case.

Another mesh study was completed using an adaptive mesh algorithm in COMSOL. This algorithm builds a mesh based on the estimated error of residuals in each element of the mesh. It automatically refines areas of the domain, such as near boundaries, where more computations are required to accurately estimate the solution. In COMSOLTM, the algorithm first computes the

Table 3.5: Number of elements in each manually-generated mesh case

	Total Mesh Elements	Mesh Elements in PTL	Mesh Elements in CL
Coarse Mesh	5912	4124	1788
Fine Mesh	14462	9078	5384
Finest Mesh	16009	9821	6188

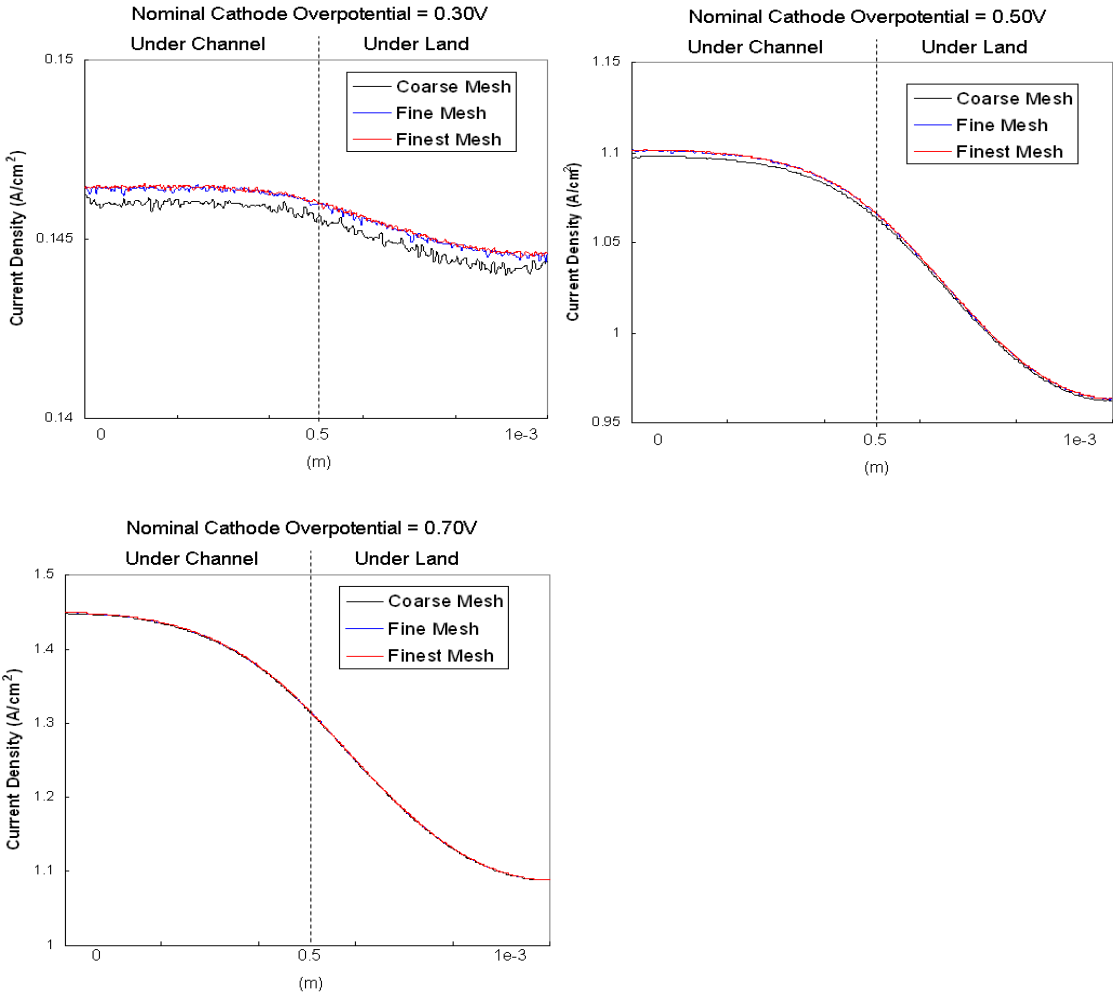


Figure 3.8: The current density distribution (A/cm^2) between the catalyst layer and membrane at a NCO of a) 0.3V b) 0.5. c) 0.7 for three mesh cases, a base case of ~ 6000 elements, a finer mesh case of ~ 14000 elements and a final case at ~ 16000 elements. At an NCO of 0.5 V, there is little difference between the three cases; the finest mesh case is slightly higher. At an NCO of 0.7V there is no discernable difference between the three cases.

solution using the most-recently-generated mesh and local error indicators are estimated on each element. Local refinements are made on the mesh based on these results. Refinements are performed on elements where the estimated error is the greatest. The total error over the domain is minimized while ensuring that the total number of elements is increased by a user-selected factor. The model is then solved again using the new mesh. The algorithm is terminated if the number of specified refinements or the maximum number elements is reached, or after the error

estimates are sufficiently small. The current model was set to terminate after three refinements and a very large maximum number of elements (10 million). The number of elements was set to increase by a factor of 1.5 in the coarse adaptive mesh case and 1.8 in the fine adaptive mesh case. The number of elements varied in each case, varied depending on the simulated conditions. In the coarse adaptive mesh case, the number of elements was between 8000 and 9500, and in the fine adaptive mesh case the number of elements was between 10500 and 13500. As well, the “longest method” in COMSOL™ was used to refine the triangles by bisecting them along the longest edge. These settings were found to give good results without leading to memory overflow issues. The predicted current density plots using this adaptive mesh algorithm are shown in Fig 3.9.

There is no discernable difference between the adaptive mesh cases. However, compared to the non-adaptive meshes there is, at most, a 0.70% error difference between the cases. At NCOs of 0.30 V and 0.50 V the adaptive mesh is shown to generate the most smooth and reliable results. Using a non-adaptive mesh, one that is generated manually, the solution appears to fluctuate at the catalyst layer / PTL boundary, and it is questionable whether convergence has been reached. The unstable behavior is shown to decrease using a finer mesh and, in the adaptive-mesh case, a smooth profile results. It appears that the adaptive mesh algorithm refined the mesh in this region to generate smaller numerical errors. Qualitatively, the plots show similar profiles, aside from the numerical fluctuations. The adaptive mesh algorithm (fine mesh case) was used for the remaining results in this thesis, as it was shown to provide the most reliable solution estimates.

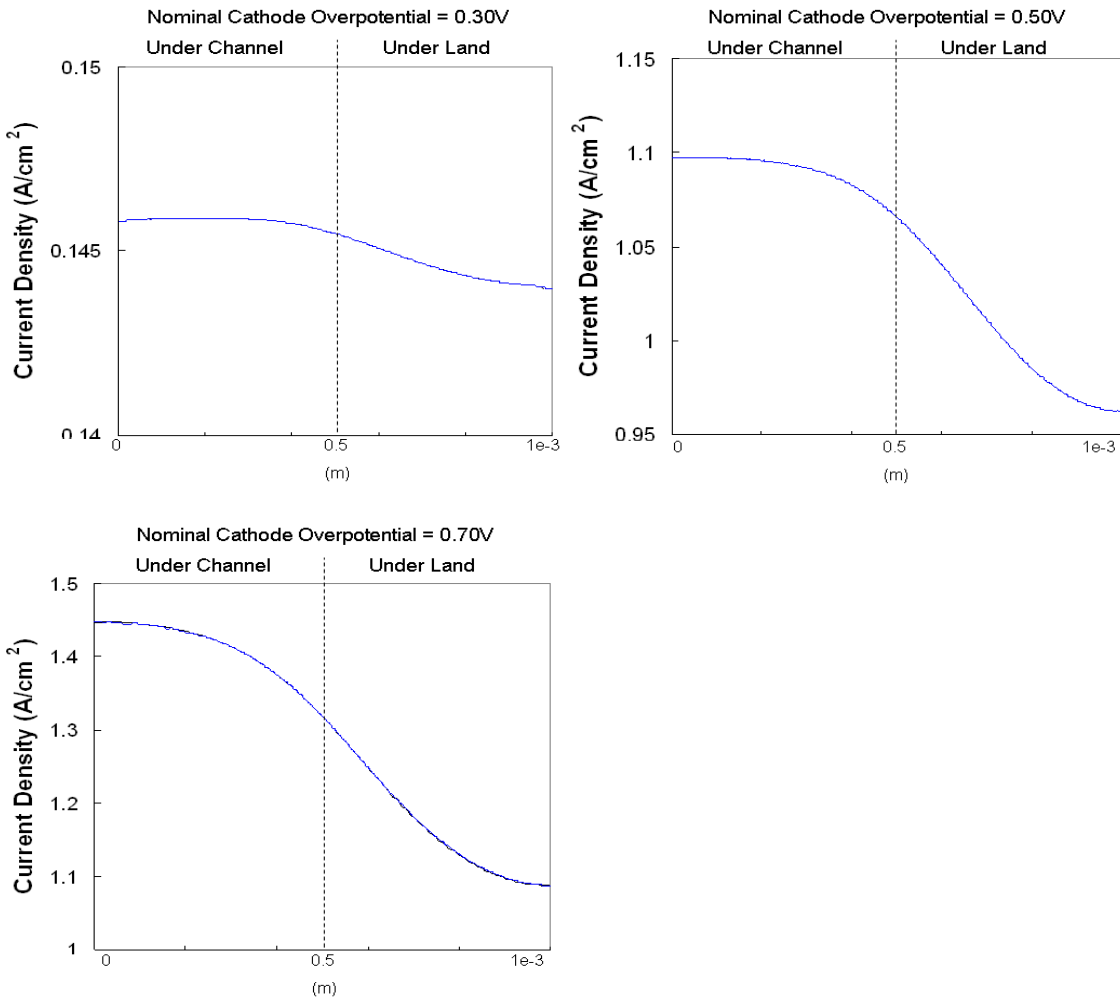


Figure 3.9: The current density distribution (A/cm^2) between the catalyst layer and membrane at a NCO of a) 0.3V b) 0.5. c) 0.7 for two adaptive mesh cases, a coarse case of 8000 to 9500 elements, a fine case of 10500 to 13500 elements. Each of the curves is coincidental and there is no discernable difference between the cases.

3.6 Error Analysis

FEM is a method to approximate the solution to partial differential equations. Since the solutions are approximations, a certain amount of error is associated with the calculations. It is important to analyze the solution to determine the reliability of the results. At the same time, it is important to consider the typical magnitudes of measurement errors that would be encountered for the dependent variables, such as the potentials and concentrations. Typically a potentiostat will measure voltages and currents within 0.1% of its range (Solatron Analytical, 2008). For example, a potentiostat that can measure up to 5A will have an error of ~0.005 A. As well, oxygen analyzers have an error of 0.1% of their full range (0.1-100% oxygen composition) in a gas stream (Nuvair, 2008). The grid study showed that there at most a 0.7% error between the different mesh cases. However, it is difficult to measure the output variables within the catalyst layer, such as oxygen concentration. Therefore, the accuracy of the solutions is appropriate, but if more accurate results are required a finer grid, with a larger solution time, could be selected.

Changing the Initial Guesses

There are several methods to analyze the reliability of the solution. One method involves using multiple initial guess to ensure that the simulation converges to the same solution. Initial guesses of the dependent variables provide a starting point for COMSOL to obtain the source terms in the PDEs. The initial guesses affect the results of the first iteration, and then COMSOL continues to iterate until convergence criteria have been met. The same solution should be arrived at for any reasonable initial guess. The following adjustments were made to the initial guesses to test whether COMSOL would converge to the same solution. The first case involved changing the initial guesses of the gas component concentrations, oxygen, nitrogen and water. The

concentrations were either doubled or halved from, 9.18 to 4.59, 34.56 to 17.265 and 6.97 to 13.49 mol / m³, respectively. In the next case, the initial guess of the electronic potential was adjusted from 0.00 to 0.05 V and the ionic potential from 0.05 to 0.10 V. A current density plot at an NCO of 0.50 V is shown in Fig 3.10 for each case, including the base case. There is no difference between the cases; the overpotential profiles were exactly the same, with no error in five significant figures. The estimated solution appears to be satisfactory based on this analysis.

Species Balances

An additional method to verify the solution is to perform overall material balances based on the estimated solution. One can examine the domain boundaries and ensure that oxygen, electrons, etc are conserved in the simulation and significant error has not been introduced into the computations. The flux of oxygen at the channel boundary should be equal to the flux of oxygen through the PTL / CL interface and should correspond to the oxygen consumed in the catalyst layer. Similar analysis was applied to each of the species in the simulation and is presented in Table 3.6. There is no significant discrepancy between the flux of species transported through the boundaries and that rate of consumption or production in the catalyst layer for each species. The largest error is between the flux of electrons at the land boundary and flux at the PTL / CL boundary (1.59%).

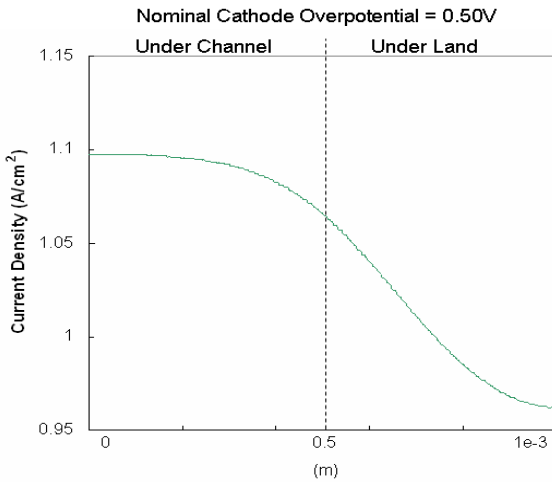


Figure 3.10: The current density distribution (A/cm^2) between the catalyst layer and membrane at a NCO of 0.5 V. A base case is shown using an adaptive mesh, as well two additional cases where the initial guess of the concentrations and potentials are changed. The simulation results were the same in each case and current density distributions are the same. An adaptive mesh was used in each case.

Residuals

In FEM, approximations of the differential equations are necessary to compute an approximate solution. One method to determine the accuracy of FEM is to examine the residuals. In general, residuals are obtained by substituting the approximate solutions into the original equations. If the equations are rearranged and set equal to zero, the residuals are the non-zero value that results from substituting the approximate solution to the dependent variables. The residual would be zero if the true solution were known. COMSOL™ provides the residuals for each element in the mesh and is shown in Fig 3.11 for a NCO of 0.30 V using an adaptive mesh. The residuals are shown to be in the magnitude of 10^{-19} , and are insignificant compared to the numerical values of the simulated variables. Residual plots were examined for the other species and the residuals were found to be of the same order of magnitude.

Table 3.6: Material balances on chemical, electronic and ionic species. The flux through four separate boundaries of the domain is given. Values are taken at a NCO of 0.30V and using an adaptive mesh.

	Channel or Land	PTL / Catalyst Layer	Catalyst Layer / Membrane	Consumed / Generated in Catalyst Layer	Units
O ₂	2.683384e-5	2.720495e-5	-	2.720557e-5	mol/m s
H ₂ O	8.586874e-5	8.70562e-5	-	8.705782e-5	mol/m s
e ⁻	10.335016	10.49975	-	10.499935	A/m
H ⁺	-	-	10.468201	10.499935	A/m

A 2-D cathode model was presented in the preceding chapter. Several improvements were made to the model, including new kinetic parameters, anisotropy of the PTL and including concentration polarization effects. Three separate mesh cases were analyzed to test grid independence. All three cases provided close results, however the adaptive mesh reduced numerical fluctuations at the PTL / CL boundary. The adaptive mesh was used in the remainder of the simulations in this thesis. An error analysis was conducted using the simulation results and the predicted results were found to be numerically reliable.

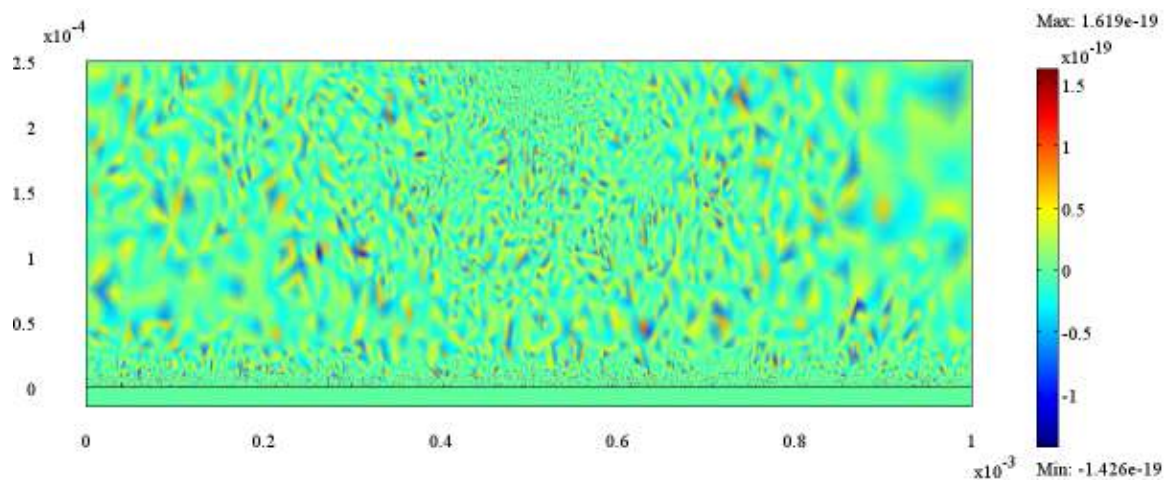


Figure 3.11: Residual plot of oxygen concentration at an NCO of 0.30 V for an adaptive mesh.

Residuals range from $-1.426e^{-19}$ to $1.619 e^{-19}$.

Chapter 4

Reaction Order Analysis

4.1 Background

Recently, the reaction order of the cathode half-reaction in a PEMFC was determined by Neyerlin *et al.* (2006) to be *one-half* with respect to the partial pressure of oxygen. This is contrary to conclusions by previous researchers (e.g., Parthasarathy *et al.*, 1991) who determined that the reaction order is *one*. The true reaction order of the ORR could remain a subject of debate in the years to come and the experiments that will be required to resolve this issue are not central to this thesis. Rather, the objective of the current work is to simulate the difference in polarization behavior of PEMFC cathodes for first- and half-order kinetic models, so that the influence of reaction order on PEMFC performance can be better understood. To this end, the 2-D PEMFC cathode model described in Chapter 3 was modified to implement the half-order kinetics. This seemingly simple modification requires significant effort because an analytical expression for Thiele modulus (for half-order kinetics) is not available. Furthermore, the appropriate expressions for the reaction rate constant and the effectiveness factor for the oxygen reduction reaction are dependent on the reaction order. Separate exchange current densities are also required for the first- and half-order models. The exchange current density is coupled with the reaction order and appropriate values are required for each model. The platinum surface area is kept constant between the first- and half-order models. This chapter presents the modifications made to the cathode model described in Chapter 3 along with an analysis of simulation results for the half-order and first-order models.

4.2 Thiele Modulus for Half-Order Reaction

Analytical expressions for the effectiveness factor, in terms of the Thiele modulus are available for zero-, first-, second-, and third-order reactions; however, such an expression for a half-order reaction does not exist. In 1965, Glaser and Rousar published an article in which they calculated the rate of a catalytic reaction with a half-order dependency on the reactant concentration. Their derivation was based on work originally completed by Thiele (1939) for reactions that exhibited a first-order dependency. Glaser and Rousar performed a mass balance on a catalyst particle, where reactants were assumed to enter a cylindrically-shaped pore at both ends, and species mass transport was governed by Fick's law, with reactions occurring on the wall of the pore. Pour and Kadlec (1968) modified this analysis to account for spherical catalyst particles. They performed a mass balance on a shell of thickness dr in the spherical particle to obtain:

$$\left(\frac{d^2c}{dr^2} \right) + \left(\frac{2}{r} \right) \left(\frac{dc}{dr} \right) = \frac{kc^{1/2}}{D_{eff}} \quad (18)$$

where r is the distance from the centre of the sphere. Eq. (18) can be written in terms of the Thiele modulus (Φ) and dimensionless groups as:

$$\frac{d^2C}{dR^2} + \left(\frac{2}{R} \right) \left(\frac{dC}{dR} \right) = \Phi^2 C^{1/2} \quad (19)$$

where, $C=c/c_s$ is the dimensionless concentration, relative to the reactant concentration at the particle surface where $r=\mathfrak{R}$. R in Eq. (19) is the dimensionless distance from the centre of the particle ($R=r/\mathfrak{R}$). The Thiele modulus Φ for the half-order reaction is defined as:

$$\Phi = \frac{d}{2} \sqrt{\frac{k_c}{(C_{O2,I/s})^{0.5} D_{eff}}} \quad (20)$$

Unfortunately, there is no analytical solution for Eq. (19).

4.3 Effectiveness Factor

A convenient analytical expression for the effectiveness factor of a first-order reaction is shown in Eq. (14). For a half-order reaction, a numerical solution of Eq. (19) was reported by Pour and Kadlec. Values of the effectiveness factor that correspond to particular values of the Thiele Modulus are presented in Fig. 4.1.

Recently, Lee and Kim (2006) developed a method to approximate the effectiveness factor for a reaction of any order and different catalyst shapes (spherical, infinite slab and infinite cylinder). Separate expressions were developed for small and large Thiele modulii. The following expressions were obtained from their method for a reaction order of *one half* and a spherical catalyst.

$$E_r = \frac{3.46}{\Phi} - \frac{3.30}{\Phi^2} - \frac{1.485}{\Phi^3} \quad (21)$$

$$E_r = 1 - \frac{1}{30} \Phi^2 + \left(\frac{-3}{3780} + \frac{3}{1890} \right) \Phi^4 \quad (22)$$

Eq. (21) applies in the case of a large Thiele modulus and Eq. (22) for a small Thiele modulus. The Thiele modulus is considered small if it is below a value of approximately 4 and high if above this value. This transition value is dependent on both the order of the reaction and the shape of the catalyst.

The effectiveness factor was recalculated and compared to the original values determined by Pour and Kadlec. They were found to be accurate up to two decimal places. The Lee and Kim approximations were used in the current cathode model.

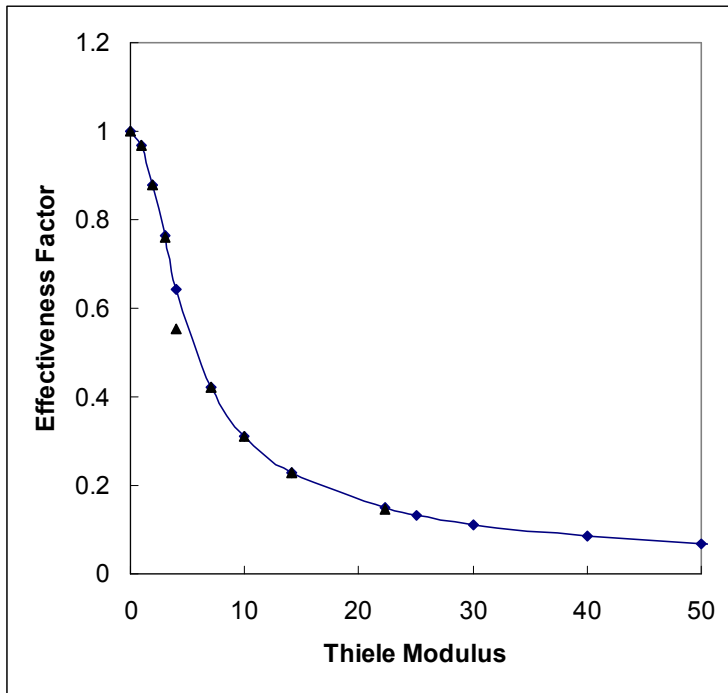


Figure 4.1: Effectiveness factor vs. Thiele Modulus for a half-order reaction. The triangular points are the results of Pour and Kadlec's numerical partial differential equation solution. The non-linear curve was plotted using equations 21 and 22 (Lee and Kim, 2006).

4.4 The Oxygen Surface Concentration at the ionomer film inner interface

For a reaction in a cathode agglomerate particle that is governed by first-order kinetics, the Thiele modulus is a function of the radius of the catalyst particle, the reaction rate constant and the effective diffusion coefficient of the reactant through the particle (Eq. 13). On the other hand, the Thiele modulus for a reaction governed by half-order kinetics is dependent on an additional parameter, the concentration on the inside surface of the ionomer film that surrounds the agglomerate particle, $C_{O_2, l/s}$ (See Fig. 2.2 and Eq. 20). To obtain an expression for $C_{O_2, l/s}$ a mass balance was performed on the ionomer film surrounding an agglomerate particle. Oxygen

diffusion through the ionomer depends on the concentrations on each side of the ionomer layer, $C_{O2,l/s}$ and $C_{O2,g/l}$. The oxygen that is transported through the ionomer film is consumed in the central portion of the agglomerate where the catalyst is located. For a half-order reaction, the reaction rate expression is:

$$R_{O2} = E_r k_c (C_{O2,l/s})^{0.5} (1 - \varepsilon_{CAT}) \quad (23)$$

Since the rate of oxygen diffusion in through the thin polymer film is equal to the rate of oxygen consumption under steady-state operation, the following is true:

$$a_{agg} D_{O2-Nafion} \frac{C_{O2,g/l} - C_{O2,l/s}}{\delta} \frac{r_{agg}}{r_{agg} + \delta} = E_r k_c (C_{O2,l/s})^{0.5} (1 - \varepsilon_{CAT}) \quad (24)$$

Rearranging Eq. (24) results in the following equation

$$C_{O2,g/l} - E_r k_c (C_{O2,l/s})^{0.5} (1 - \varepsilon_{CAT}) \frac{(r_{agg} + \delta)\delta}{a_{agg} Dr_{agg}} - C_{O2,l/s} = 0 \quad (25)$$

All variables in Eq. (25) are known state variables that are calculated in the PEMFC model, except for $C_{O2,l/s}$. Since E_r is a complex function of Φ and $C_{O2,l/s}$ (Eqs. 21 and 22), it is not possible to solve Eq. (25) analytically for $C_{O2,l/s}$. However, it is possible to solve this implicit algebraic equation as a pseudo-PDE in COMSOL™ using a general-form PDE option. To solve Eq. (25) along with the model PDEs using COMSOL™, all the coefficients for the partial derivative terms were set to zero and Eq. (25) is set as the source term. Values for the Thiele Modulus and effectiveness factor can now be determined by adding this general form PDE to the original set of PDEs.

4.5 Reaction Rate at the Catalyst Surface

The reaction rate within the catalyst layer is a sink term in the PEMFC model that describes the electrons, protons and oxygen that are consumed (and the water that is generated). The consumption of electrons in the catalyst layer (and the consumption of oxygen) is described in Table 3.2 and is derived from expressions for the reaction rate inside the agglomerate particles and for oxygen transport through the ionomer film to the catalyst. In a half-order reaction model, the expression for oxygen transport through the film is the same as that for the first-order model, however, the rate of consumption of reactants (i.e. electrons, protons and oxygen) depends on the concentration of oxygen to the power of *one-half* instead of *one*. The oxygen flux through the catalyst layer for a half-order reaction is calculated as:

$$j_{O_2} = E_r k_c (C_{O_2,l/s})^{0.5} (1 - \varepsilon_{CAT}) \quad (26)$$

As well, the diffusive through the catalyst layer can be written in terms of the oxygen concentration on both sides of the ionomer film:

$$j_{O_2} = \frac{(C_{O_2,g/l} - C_{O_2,l/s})}{\delta} \times \frac{r_{agg} Da_{agg}}{(r_{agg} + \delta)} \quad (27)$$

Eq. (26) is rearranged to solve for $C_{O_2,l/s}$ and substituted into Eq. (27).

$$j_{O_2} = \frac{r_{agg} Da_{agg}}{(r_{agg} + \delta) \delta} \left(C_{O_2,g/l} - \frac{(j_{O_2})^2}{[E_r k_c (1 - \varepsilon_{cat})]^2} \right) \quad (28)$$

The resulting quadratic is solved and is used as the sink and source terms for the gaseous, electron and proton transport differential equations in COMSOLTM.

4.6 Kinetic Influence on Cathode Performance

Before running detailed simulations in COMSOLTM, the influence of the half-order kinetics was examined using the Tafel equation:

$$i = i_0 \left(\frac{C_{O2}}{C_{O2ref}} \right)^\gamma \exp \left(-\frac{\alpha_c nF}{RT} \eta_{local} \right) \quad (29)$$

This examination (see Fig. 4.2) enabled study of how the current density is affected by the change in the exchange current density and the reaction order alone, when no transport effects are present. Subsequently, a complete cathode simulation was performed using COMSOLTM in order to simulate the combined influence of the half-order kinetics and the transport phenomena in the cathode on fuel cell performance (See Figs 4.3 to 4.4). While examining the influence of reaction order on current density using the Tafel equation alone, an oxygen concentration of 9.18 mol/m³ (corresponding to air with 50% RH at a temperature 80°C and an oxygen partial pressure of 0.177 atm) was assumed at the catalyst sites. The overpotential was varied between 0.1 and 0.8 V to obtain a range of corresponding current densities, which are shown in Fig. 4.2. The half-order-reaction model predicts a lower current density than the first-order-reaction model. The smaller exchange current density used in the half-order-reaction model is largely contributing to this result. The reaction order parameter, γ , also affects the current density. Figure 4.2 indicates that changing the reaction order from *one* to *one half* should decrease the predicted current density in the full COMSOL simulation.

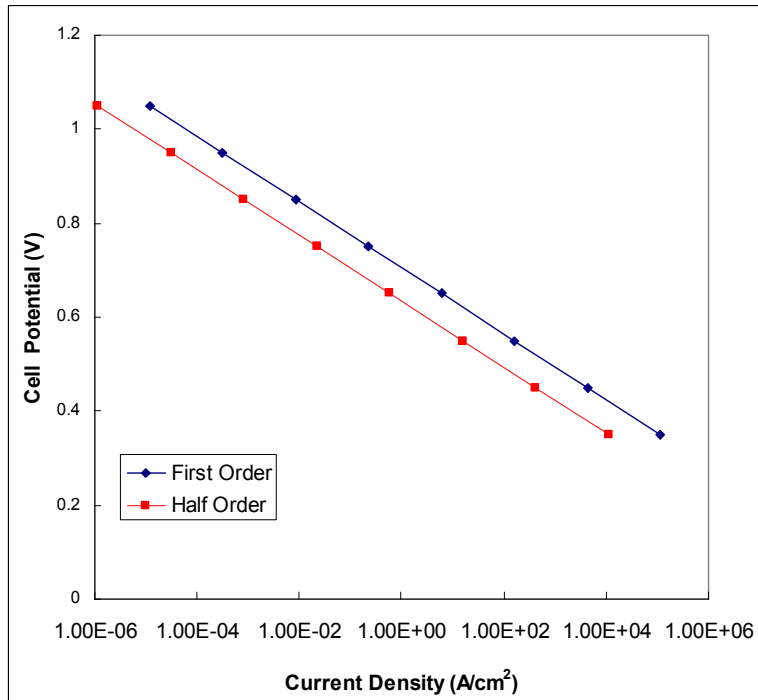


Figure 4.2: A comparison of the current density distribution using the Tafel equation for cell potentials between 0.3 and 1.1 V. First-order and half-order models are compared.

4.7 Solution Method (Half-order Reaction)

The revised cathode model with half-order kinetics was implemented in COMSOLTM. The transport equations listed in Table 3.1, which describe the transport of each species in the PTL and catalyst layer, were used in model. The corresponding source terms are listed in Table 3.2. The quadratic formula was applied to Eq. 28 to solve for the oxygen flux used to derive each source term. The positive real root was used to calculate each source term. As well, a general form PDE was added to the set of PDEs in order to enter Eq. (25) implicitly. The modifications to the effectiveness factor and Thiele modulus were applied. Eqs. (21) and (22) derived from Lee and Kim (2006) were used to calculate the effectiveness factor.

The iterative, stationary, nonlinear solver in COMSOLTM was used to solve the model. A relative tolerance of $1.0e^{-6}$ was set as the criterion for convergence. The adaptive mesh algorithm was applied to the simulations, as it was shown in Chapter 3 to provide reliable results. In each simulation case, the ionic potential at the membrane boundary z_0 , (i.e. the NCO) was varied using a parametric version of the solver, wherein the potential was incremented and the model was solved, using the numerical solution from the calculations with the previous potential as the initial guess. Unfortunately, at high NCOs, (above 0.50 V), the COMSOLTM simulations converged to an unrealistic (negative) values for $C_{O2,l/s}$, using an increment of 0.05 V for each subsequent iteration. To arrive at the correct solution for $C_{O2,l/s}$ smaller increments were required to provide a more accurate starting point for the subsequent iteration. Convergence to the correct numerical solution was obtained when the potential was incremented by 0.025 V for each subsequent solution, resulting in more simulation points than were used in the first-order case.

4.8 Results and Discussion

A polarization curve comparing a first- and half-order reaction is shown in Fig. 4.3. At high potentials (above 0.6 V) the first-order model predicts a higher current density than the half-order model. However, below 0.6 V, the half-order model predicts better performance. Note that k_c is a function of the exchange current density, i_0 , and a value of $3.85 \times 10^{-4} \text{ A/m}^2$ (Parthasarathy *et al.*, 1992a) was used in the first-order model. However, Neyerlin *et al.* calculated an exchange current density of $1.50 \times 10^{-4} \text{ A/m}^2$ (more than half that of the first-order case), for the same oxygen partial pressure. k_c is directly proportional to i_0 , hence the reaction rate or current density is lower in the initial portion of the polarization curve.

At higher current densities the performance of the cell is largely limited by oxygen diffusion in the catalyst layer. A half-order reaction is less dependent on the oxygen concentration than a first-order reaction and should not result in as large a current drop due to oxygen limitations. To closely examine the difference between the half-order and first-order simulation results, current density distributions were determined at 0.3V, 0.5V and 0.7 V, as shown in Fig. 4.4. At an NCO of 0.3 V the current density under the channel (at the membrane-catalyst interface) of the first-order case (0.145 A/cm^2) is more than double that for the half-order case (0.066 A/cm^2). The current density is slightly higher under the channel in each case. Oxygen diffusion and electron transport were not significantly hindered at an NCO of 0.3 in the first-order case. Modifying the model, so that it assumes a half-order reaction, does not change these qualitative results. At a NCO of 0.5 V the average current density of the first-order case and half-order case are nearly equal. The first-order reaction has a larger current density than the half-order case, under the channel. While under the land the half-order case has a higher current density. At 0.7 V the half-

order case performs better by an average of 0.02 V. Qualitatively, both distributions experience a maximum current density under the channel.

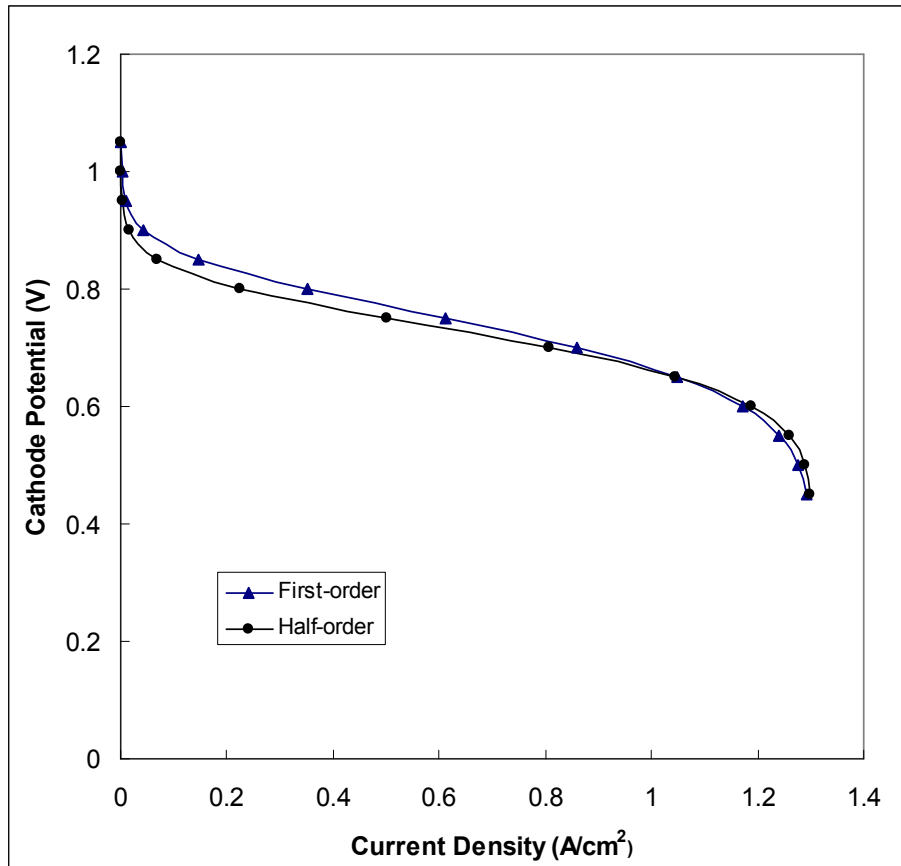


Figure 4.3: Predicted polarization curves of the PEMFC cathode model for cases where a first-order and half-order reaction is assumed. An adaptive mesh was used in each case.

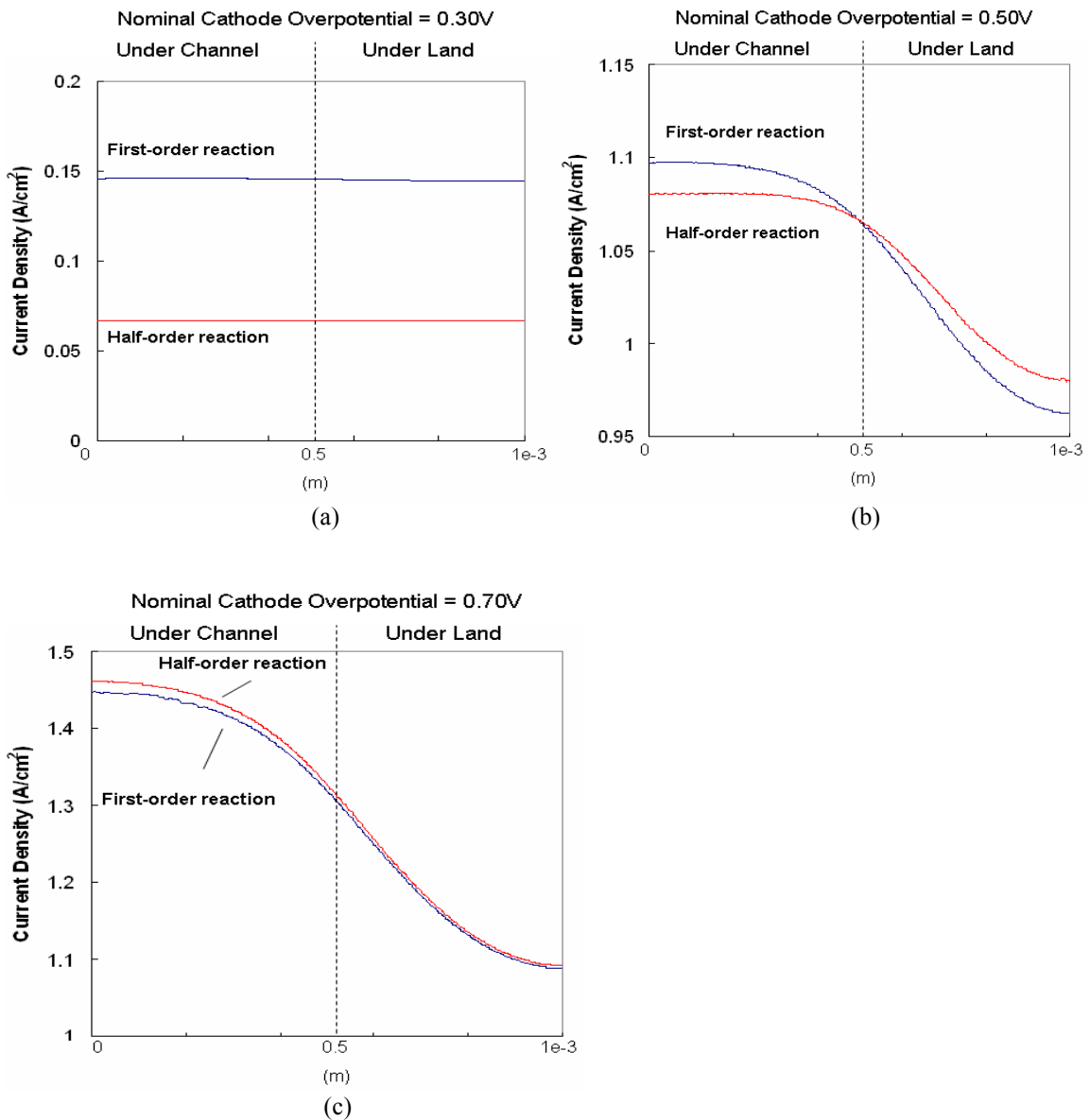


Figure 4.4: The current density distribution (A/cm^2) between the catalyst layer and membrane at a NCO of a) 0.3V b) 0.5. c) 0.7 Cases for a first-order and half-order reaction are presented. An adaptive mesh was used in each case.

Contour plots of the oxygen reaction rate were created at NCOs of 0.30, 0.50 V and 0.70 V and are shown in Fig. 4.5 a), b) and c) respectively. At a NCO of 0.30 V the reaction rates of the first-order case is significantly higher than the half-order case, mirroring the results from the current density profiles. In both cases the reaction rate is higher near the membrane boundary due to higher ionic transport limitations at this NCO. In fact, the electronic conductivity in the catalyst layer (100 S/m) is two orders of magnitude higher than the ionic conductivity. As well, in the first-order case and near the membrane boundary, higher reaction rates are experienced under the channel because of oxygen transport limitations. However, near the PTL/CL interface the maximum reaction rate is under the land that shows that electronic transport is limiting in this region of the CL. In the half-order case this phenomenon is not evident as the reaction rate is not as dependent on the oxygen concentration as the first-order case.

In Fig. 4.5 b) at 0.5 V, again the higher reaction rates are experienced near the membrane boundary, rather than the PTL/CL interface. However, oxygen limitations are more severe at this NCO, as evidenced by the larger reaction rate gradients near the membrane boundary. At 0.70 V the contour plots of the first- and half-order reaction are similar in both magnitude and the contour distributions. At this NCO the oxygen reaction rate is highest under the channel, as oxygen transport limitations are dominant in both cases.

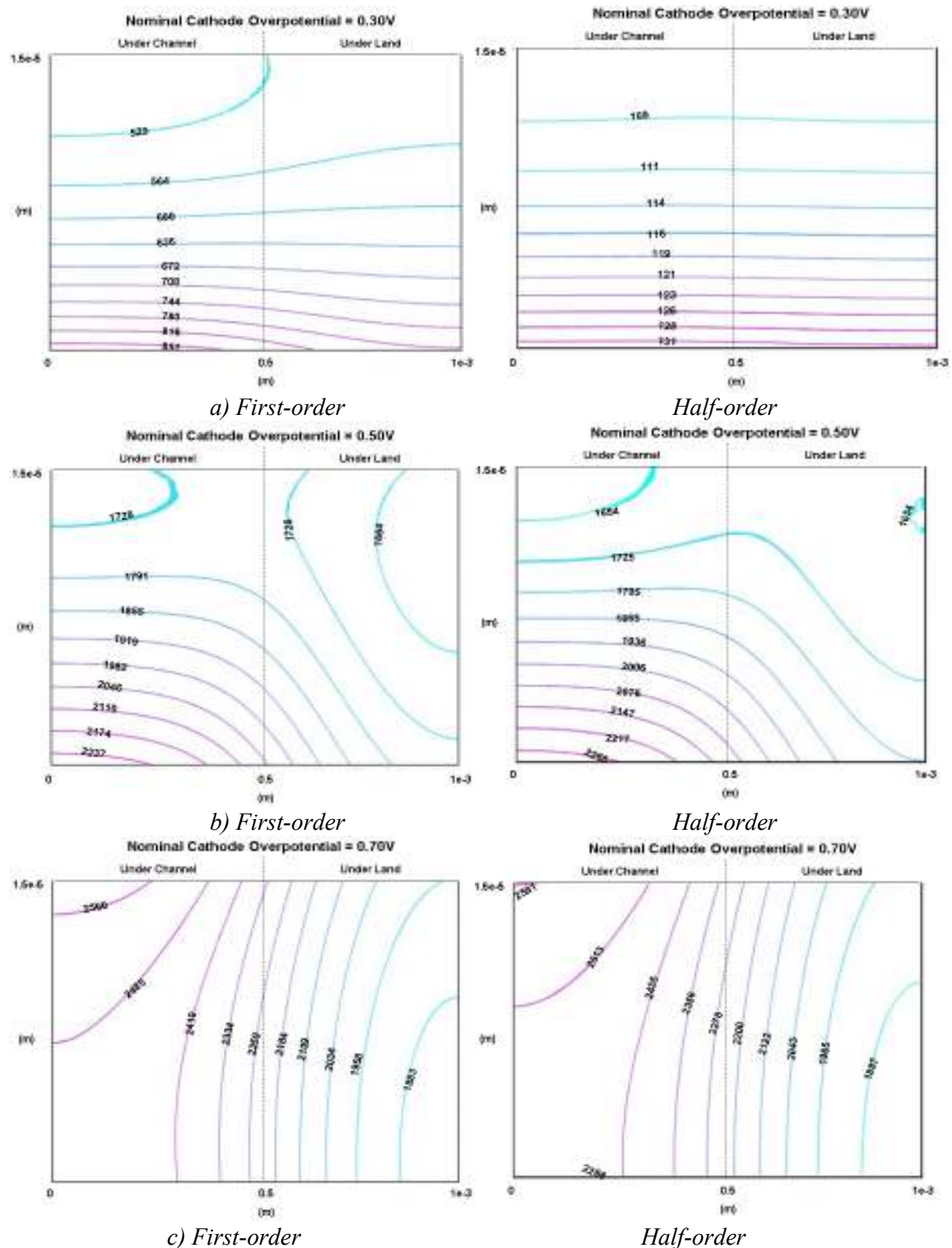


Figure 4.5: The oxygen reaction rate profile ($\text{mol}/\text{m}^3/\text{s}$) in the catalyst layer for a NCO of a) 0.3V b) 0.5V c) 0.70V. Cases for a first-order and half-order reaction are presented. An adaptive mesh was used in each case.

4.9 Results and discussion for first and half-order models under varying oxygen concentrations

In a fuel cell, the oxygen concentration can vary significantly along the length of the serpentine channel within each cell due to oxygen consumption and water generation. The oxygen concentration (or mole fraction) at the channel boundary was varied in the model to examine the influence of changing oxygen concentration in the channel on both the first and half-order reaction models. The oxygen mole fraction was adjusted in each case, and the corresponding nitrogen and water mole fractions were calculated using the stoichiometry of the cathode half-reaction. The mole fractions and concentrations are listed in Table 4.1 for three cases, a high oxygen concentration, based on the current simulations (case 1) shown in Figs. 4.3 and 4.4 and two cases using lower concentrations of oxygen, 6.99 and 4.81 mol/m³ (cases 2 and 3, respectively), at the channel/PTL boundary. Polarization curves generated for NCOs between 0.05 and 0.70 V are shown in Figs. (4.5) and (4.6).

Table 4.1: Chemical species concentrations at the channel/PTL boundary for case 1 (base case), case 2 (mid-oxygen concentration) and case 3 (low oxygen concentration).

	Species	Mole Fraction (-)	Concentration (mol/m ³)
Case-1	O ₂	0.177	9.18
	N ₂	0.667	34.56
	H ₂ O	0.156	8.02
Case-2	O ₂	0.135	6.99
	N ₂	0.643	33.30
	H ₂ O	0.221	11.48
Case-3	O ₂	0.0929	4.81
	N ₂	0.619	32.06
	H ₂ O	0.288	14.90

The polarization curves in Figs (4.6) and (4.7) clearly show a decrease in fuel cell performance with decreasing oxygen concentration, as expected. The limiting current density at the catalyst layer / membrane interface decreases (from ~ 1.3 to ~ 1.0 and $\sim 0.7 \text{ A/cm}^2$) in the first-order case. A similar trend is also shown in the half-order case. In Table 4.2 the relative decrease in current densities for each case is listed, as this information is not easy to discern from a polarization curve. In all cases the largest changes in current densities between the low-oxygen cases and the base case are realized at low and high overpotentials, rather than near 0.5 V. For example, in Case 2, for the first-order model the relative decreases in the current density from the base case, for NCOs of 0.05, 0.30 and 0.70 V, are 30.3, 18.7 and 23.6%, respectively. At low overpotentials activation losses, which are dependent on the oxygen concentration at the catalyst sites (see

Table 4.2: Relative decrease in current density of case 2 and 3 in comparison to the base case for the first- and half-order reaction models.

NCO (V)	First-Order Kinetics		Half-order Kinetics	
	Case 2 (%)	Case 3 (%)	Case 2 (%)	Case 3 (%)
0.05	30.36	56.35	19.35	39.06
0.10	30.31	56.33	19.36	39.06
0.15	30.16	56.16	19.29	39.00
0.20	29.34	55.39	19.04	38.70
0.25	26.07	52.13	17.85	37.31
0.30	18.68	43.74	13.38	32.05
0.35	12.10	35.49	6.87	23.59
0.40	11.82	35.07	3.55	23.36
0.45	14.93	38.39	10.14	32.53
0.50	18.26	41.75	16.04	39.37
0.55	20.86	44.16	20.16	43.54
0.60	22.41	45.58	22.40	45.60
0.65	23.24	46.32	23.37	46.46
0.70	23.65	46.67	23.74	46.77

Section 4.6), are dominant. Therefore it is expected that a drop in oxygen concentration (the average concentration, $CO_{2,l/s}$, at the PTL/CL boundary for the half-order model at an NCO of 0.05 V is 0.869, 0.648, and 0.446 mol/m³ for case 1, 2 and 3 respectively) at the channel will lead to a drop in current density, even at low NCOs.

At an NCO of 0.40 V the relative influence of oxygen concentration on the predicted fuel cell performance is at its lowest, 12% and 35% for cases 2 and 3, respectively, and 3.5% and 23% current density drops for first- and half-order cases, respectively. An NCO of 0.40 V corresponds to the ohmic-loss region of the polarization curve where ohmic losses are expected to constitute the majority of the overpotential losses. Ohmic losses are dependent on electronic and ionic transport; therefore oxygen concentration will not influence the predicted performance significantly, relative to low NCOs. At high overpotentials mass transport limitations are dominant; therefore the predicted current density should see a significant decrease at lower oxygen concentrations. The concentration of oxygen at the agglomerate surface, $C_{O2,l/s}$ drops significantly at high overpotentials (as shown in Fig 4.8) due to the increasingly high reaction rates required.

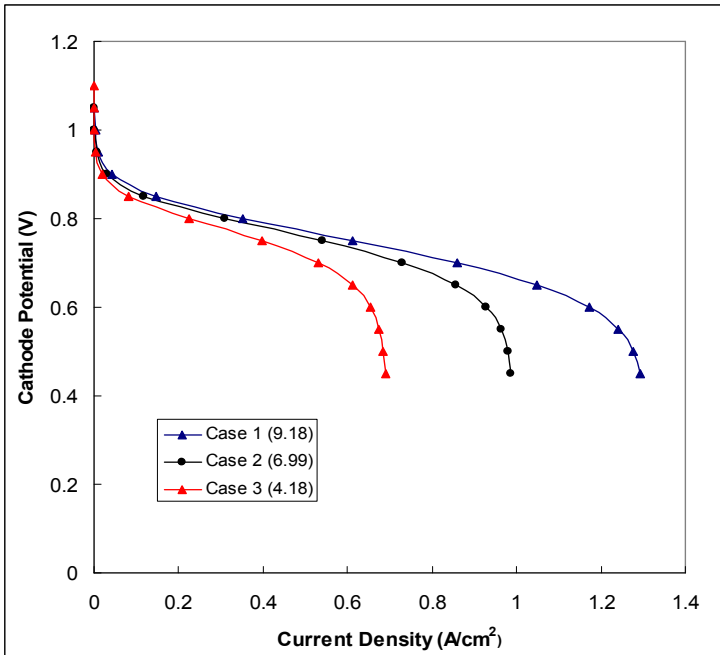


Figure 4.6: Predicted polarization curves of the PEMFC cathode model for the first-order reaction. Three cases are considered where the oxygen concentration at the channel/PTL boundary is varied, case 1 ($9.18 \text{ mol}/\text{m}^3$), case 2 ($6.99 \text{ mol}/\text{m}^3$) and case 3 ($4.18 \text{ mol}/\text{m}^3$). An adaptive mesh was used in each case.

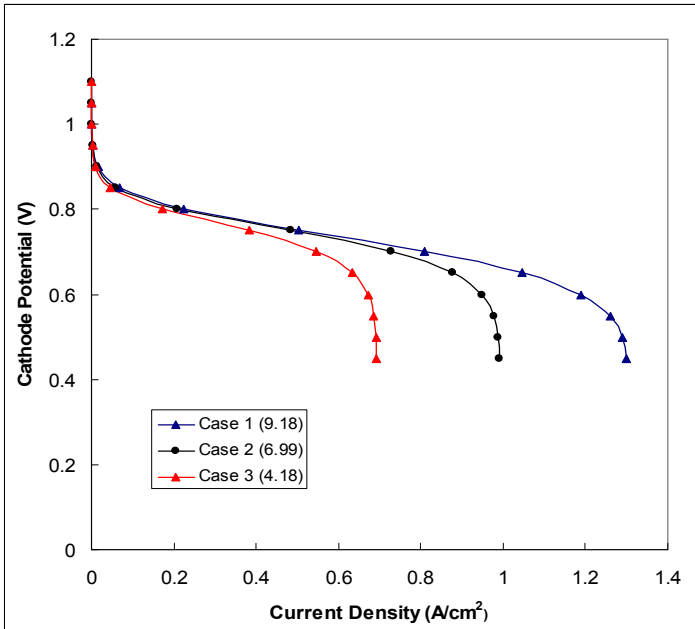


Figure 4.7: Predicted polarization curves of the PEMFC cathode model for the half-order reaction. Three cases are considered where the oxygen concentration at the channel/PTL boundary is varied, case 1 ($9.18 \text{ mol}/\text{m}^3$), case 2 ($6.99 \text{ mol}/\text{m}^3$) and case 3 ($4.18 \text{ mol}/\text{m}^3$). An adaptive mesh was used in each case.

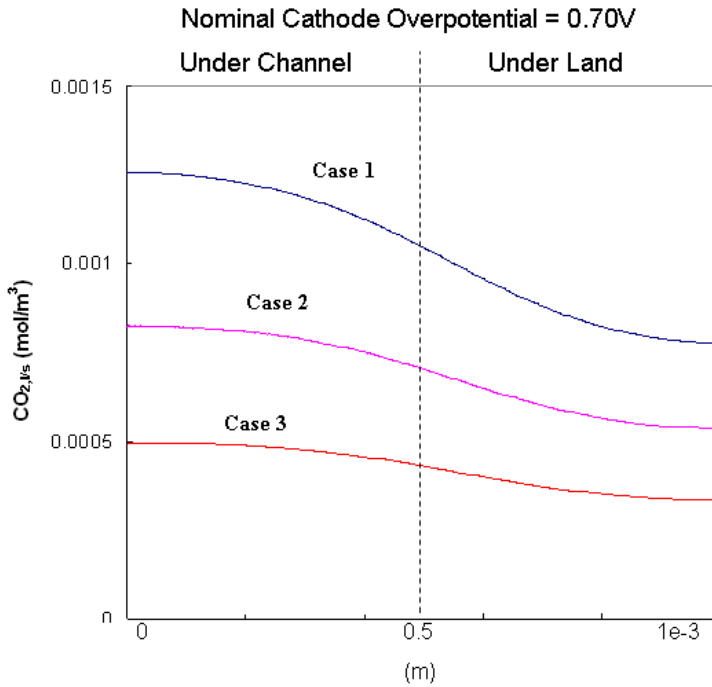


Figure 4.8: Dissolved oxygen concentration at the inside of the ionomer interface, $CO_{2,ls}$ at the PTL / CL interface. Oxygen concentration for three cases are considered where the oxygen concentration at the channel/PTL boundary is varied, case 1 (9.18 mol/m^3), case 2 (6.99 mol/m^3) and case 3 (4.18 mol/m^3). An adaptive mesh was used in each case.

The first-order and half-order cases are compared in Figs. (4.9) and (4.10). Behavior similar to that observed in the base case also occurs at lower oxygen concentrations. The predicted current density from the first-order model is higher at lower overpotentials and the discrepancy between the two cases decreases with increasing overpotential. At low NCOs (0.05V) or high cathode potentials the first-order reaction case predicts a larger current density drop than the half-order case, 30% and 56% versus 19% and 39%, respectively. The weaker dependency on oxygen concentration for the half-order case is evident in this case. The point at which the polarization curves cross each other changes when the oxygen concentration is varied. In case 3 the polarization curves cross at an NCO of ~0.42 V while in case 1 the curves cross at ~0.57 V. Mass transport limitations are more dominant in the third case (low oxygen concentration) and the

kinetic differences are not as apparent. In each case, the predicted limiting current densities of the first- and half-order reaction models are close (less than 1% difference). At higher current densities, mass transport limitations arising from diffusion through the PTL, catalyst layer and electrolyte, have a larger influence over fuel cell performance than the kinetics.

In summary, a 2-D cathode model that assumed half-order kinetics, with respect to oxygen concentration, was developed. The reaction order was shown to be an important factor in PEMFC modeling. At low overpotentials below 0.5 V, the first-order reaction model predicted higher current densities than the half-order model, while the opposite is true at high overpotentials above 0.5 V. Qualitatively, the current density profiles are similar between the first and half-order reaction cases. In addition, the oxygen concentration at the channel / PTL boundary was varied to examine the influence of oxygen concentration on the predicted fuel cell performance. A decrease in the oxygen concentration was shown to have a large influence at low and high cell potentials where activation and mass transport losses are dominant. A relatively small decrease in current density occurred in the ohmic region of the polarization curve where oxygen concentration has the least influence. In the activation region of the polarization curve, the decrease in the oxygen concentration had a larger effect on the predicted current density of the first-order model than the half-order model. As well, the limiting current density of both models was close, within 0.5%. It is worth noting that greater differences between the first- and half-order models were observed at low overpotentials where fuel cells do not normally operate. However, degradation is important in this region and these results may provide insight into this area of study. For example, it is expected that a fuel cell that follows the half-order model would experience less degradation at low overpotentials since the current density has a lower dependency on the oxygen concentration than in the first-order model.

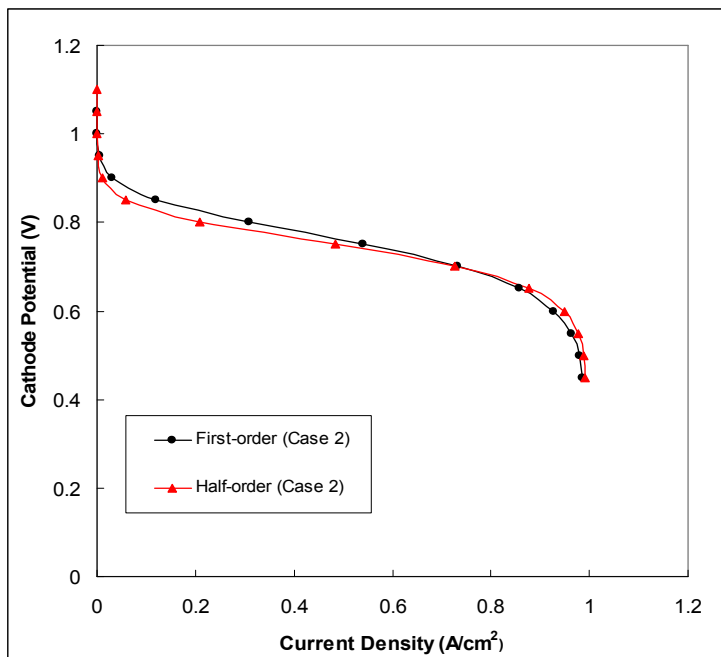


Figure 4.9: Predicted polarization curves of the PEMFC cathode model for case 2 (6.99 mol/m^3 O₂ concentration). First- and half-order cases are considered. An adaptive mesh was used in each case.

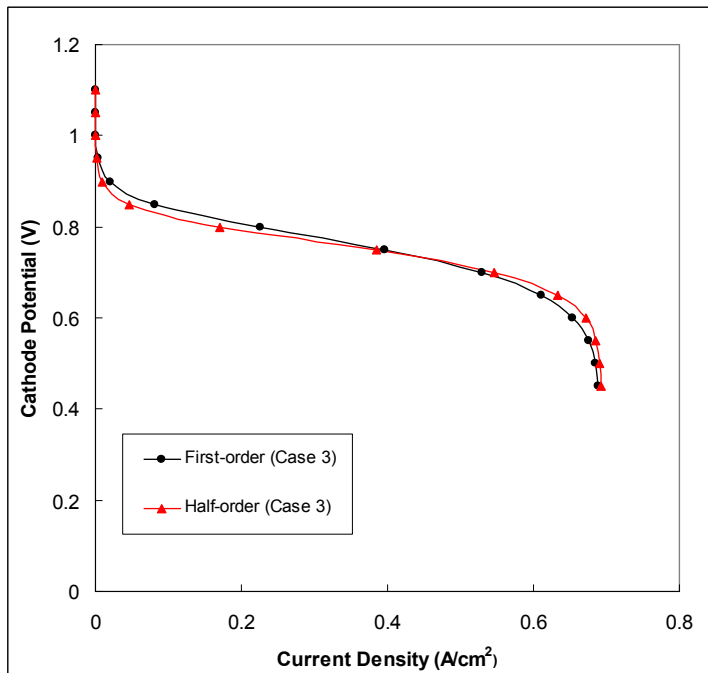


Figure 4.10: Predicted polarization curves of the PEMFC cathode model for case 3 (4.18 mol/m^3 O₂ concentration). First- and half-order cases are considered. An adaptive mesh was used in each case.

Chapter 5

Conclusions and Recommendations

5.1 Conclusions

In this study, a 2-D PEMFC cathode model is developed and the kinetic phenomena in the catalyst layer are examined, specifically the reaction order of the ORR. The model incorporates coupled transport and kinetic phenomena in the catalyst layer as well as species transport through PTL and CL sub-domains of the model. Unfortunately, the true reaction order of the ORR with respect to oxygen concentration is unknown. The main objectives of this thesis were to simulate PEMFC cathode behaviour with both first- and half-order reactions, and to examine the consequences of assuming half-order kinetics as opposed to first-order kinetics. Minor improvements and a detailed error and grid study were made before embarking on a detailed analysis of the influence of half-order reaction kinetics on PEMFC cathode performance. A list of the improvements and conclusions about their influences on model predictions are listed below, followed by conclusions from the main part of the study where cathode performance with half-order and first-order reaction kinetics is compared.

i) Minor Model Improvements:

- The kinetic parameters were adjusted to account for the revised assumption that the double Tafel slope does not arise from a change in underlying kinetics, but results from a transport issue. Significant improvements in the predicted cathode performance at NCOs above 0.3 V were observed using the new kinetic parameters corresponding to a single Tafel slope.

-Anisotropic geometry in the PTL was accounted for, because it has been shown to influence modeling results in the catalyst layer (Pharoah *et. al.*, 2006, Zhou and Lee, 2006). Including anisotropic electronic conductivity in the model resulted in higher predicted current densities, due to higher conductivities in the in-plane direction. The anisotropic diffusivities had an opposing effect on the cathode performance, particularly at NCOs above 0.6 V, because smaller diffusion coefficients were used in both the in-plane and through-plane directions.

-Finally, the model was revised to account for changes in the concentration overpotential in the catalyst layer when determining the reaction rate. It was shown that there was little impact on the predicted polarization curve or the current density plots, and there was a very small drop of about 0.01 V in the predicted performance when the influence of the concentration overpotential was included in the model.

ii) Reaction Order:

The reaction order is an important factor in PEMFC modeling. There is debate as to what is the true reaction order is for oxygen reduction in a PEMFC cathode (Neyerlin *et. al.*, 2006). Simulations were conducted using both half-order and first-order reaction kinetics so that predicted differences could be examined.

- There are several obstacles that must be resolved when modeling half-order reaction kinetics in an agglomerate cathode model. The reaction rate expression must be modified to account for a change in the reaction order. Also, suitable expressions must be obtained for the effectiveness factor and for the oxygen concentration on the inside of the ionomer film. Because it was not possible to obtain an explicit expression for this oxygen concentration, it was necessary to use the

general-form PDE feature within COMSOL, which permits the user to solve implicit algebraic equations along with the PDEs.

- The simulation results showed that the reaction order can have a significant effect on the predicted fuel cell performance. At low overpotentials below 0.5 V, the first-order reaction model predicted higher current densities that are higher (twice as high at 0.3 V), while at high overpotentials above 0.5 V the half-order case has a slightly higher current density. Qualitatively, the current density and reaction rate profiles are similar between the first and half-order reaction cases.

Concentration Effects:

The influence of oxygen concentration on the predicted fuel cell performance was examined in both the first- and half-order models. The oxygen concentration at the channel / PTL boundary was varied to simulate the effect of decreasing oxygen concentration at points downstream along the serpentine channel of a bipolar plate. The largest relative decreases in the predicted current density, at the CL / membrane boundary, were observed at low and high cell potentials where activation and mass transport losses are dominant. A decrease in the oxygen concentration from 9.18 to 6.99 mol/m³ resulted in drops of 30.3, 18.7 and 23.6% for NCOs of 0.01, 0.30 and 0.70 V, respectively. The lower oxygen concentration resulted in a relatively small decrease in current density in the ohmic region of the polarization curve where electronic and ionic transport is dominant. Between the first- and half-order models, several differences were apparent. In the activation region of the polarization curve, the decrease in the oxygen concentration had a larger effect on the predicted current density of the first-order model. As well, the limiting current

densities of both cases were close to each other (within 0.5%) since mass transport is limiting in this region of the polarization curve where kinetics are not as important.

5.2 Recommendations

1. The reaction order does have a mild influence on the predicted performance of PEMFCs and further experimental studies should be performed to determine whether it is more appropriate to assume first- or half-order reaction kinetics for oxygen consumption in PEMFC cathodes.
2. Anisotropy in electronic conductivity and gas diffusivity in the PTL should be included in future PEMFC models, because these phenomena result in significant changes to predicted fuel cell performance. In addition, anisotropy of thermal conductivity should be included in models that account for temperature variations in the PEMFC. Unfortunately, the model in this thesis assumes isothermal operation and that all water passing through the PTL and within the catalyst layer is water vapour, rather than liquid. It is well known that liquid water can be present in PEMFCs and that it can influence fuel cell performance, (Mudhusudana *et al.*, 2007). Liquid water transport in the cathode remains one of the more poorly understood phenomena in a PEMFC. Introducing the effects of liquid water into the porous transport layer and catalyst layer will allow modelers to investigate these effects in detail. An accurate model that includes the presence of liquid water will be beneficial in designing and optimizing fuel cells. Additional phenomena that will need to be included in PEMFC models that account for liquid water are: temperature distributions in the cathode, water transport from the anode and through the membrane, latent heat effects associated with evaporation and condensation of water, pressure distributions within the cathode, and two-phase flow within the porous catalyst, the PTL, and the

cathode channels. Although many researchers (Mudhusudana *et al.*, 2007, Wang *et al.*, 2006, Shah *et al.*, 2007) have begun to work on this problem, much work remains to be done.

3. Future modelers should not include double Tafel-slope correlations in their mathematical models, unless new experimental results confirm that the apparent double slope results from kinetic effects, because this type of assumption can lead to erroneous model predictions.
4. Future modelers should include the influence of concentration overpotential within the catalyst layer if they require very accurate predictions of PEMFC performance. Including this effect is not very important if only qualitative predictions are required.
5. The model predictions rely on a large number of uncertain kinetic and transport parameters. It will be important for future modelers to obtain better parameter estimates if they require good quantitative predictions from their models.

Bibliography

- Barbir, F., *PEM Fuel Cells: Theory and Practice*, Academic Press, 2005.
- Bernardi, D. and Verbrugge, M., *Mathematical Model of a Gas Diffusion Electrode Bonded to a Polymer Electrolyte*, AIChE Journal, 37(8), 1151-1163, (1991).
- Bird, R., Stewart W., and Lightfoot, E., *Transport phenomena*, John Wiley & Sons, Inc., New York, (1960).
- Broka, K. and Ekdunge, P., *Modeling the PEM fuel cell cathode*, Journal of Applied Electrochemistry, 27, 281-289, (1997).
- Damjanovic, A. and Brusic V., *Electrode Kinetics of Oxygen Reduction on Oxide-free Platinum Electrodes*, Electrochimica Acta, 12, 615, (1967).
- Fuller, T. and Newman, J., *Water and thermal management in solid-polymer-electrolyte fuel cells*, Journal of Electrochemical Society, 140(5), 1218-1225, (1993).
- Fogler, S., *Elements of Chemical Engineering*, Prentice Hall, (2006).
- Glaser, V. and Rousar, I., *Calculation of the Rate of a Half-Order Reaction Proceeding in Pores of a Catalyst*, Collection Czechoslov. Chem Commun, 31, 2137-2143, (1966).
- Hamilton, D., *A numerical experiment to determine diffusive flux coefficients for porous media*, Master's Thesis, Queen's University, (2002).
- Hsueh, K. L., Chang, H.H., Chin, D-T, and Srinivasan S., *Electrode Kinetics of Oxygen Reduction on Platinum in Trifluoromethanesulphonic Acid*, Electrochimica Acta, 30, 1137, (1985).

Jaouen, F., *Electrochemical characterization of porous cathodes in the polymer electrolyte fuel cell*, Ph.D. Thesis. (2003).

Kulikovsky, A. A., *Quasi-3D Modeling of Water Transport in Polymer Electrolyte Fuel Cells*, Journal of Electrochemical Society, 150(11), A1432–A1439, (2003).

Lee, J. and Kim, H., *An approximation method for the effectiveness factor in porous catalysts*, Chem. Eng. Sci., 61, 5127-5136, (2006).

Madhusudana, R., Bhattacharya, D., Rengaswamy, R., and Choudhury, S.R., *A two-dimensional steady state model including the effect of liquid water for a PEM fuel cell cathode*, Journal of Power Sources, (2007).

Middleman, E., *Improved PEM fuel cell electrodes by controlled self-assembly*, Fuel Cells Bulletin, 11, 9-12, (2002).

More, K.L., Borup, R. and Reeves, K.S., *Identifying contributing degradation phenomena in PEM fuel cell membrane electrode assemblies via electron microscopy*, The Electrochemical Society, 3(1), 717-733, (2006).

Murthi, V., Urian, C. and Mukerjee, S., *Oxygen reduction kinetics in low and medium temperature acidic environment: correlation of water activation and surface properties in supported Pt and Pt alloy electrocatalysts*, Journal of Physical Chemistry B, 108, 11011-11023, (2004).

Neyerlin K.C., Gu, W., Jorne, J., and Gasteiger H., *Determination of Catalyst Unique Parameters for the Oxygen Reduction Reaction in PEMFC*, J.E.S, 153(10), A1955-A1963 (2006).

Nuvair, www.nuvair.com, (2008).

Parthasarathy, A., Srinivasan, S., Appleby, A. and Martin, C., *Pressure dependence of the oxygen reduction reaction at the platinum microelectrode/Nafion interface: electrode kinetics and mass transport*, Journal of the Electrochemical Society, 139(10), 2856-2862, (1992a).

Parthasarathy, A., Srinivasan, S., Appleby, A. and Martin, C., *Temperature dependence of the oxygen reduction reaction at the platinum microelectrode/Nafion interface: electrode kinetics and mass transport*, Journal of the Electrochemical Society, 139(9), 2530-2537, (1992b).

Paulus, U.A. et. al., *Oxygen reduction on carbon-supported Pt-Ni and Pt-Co alloy catalysts*, Journal of Physical Chemistry B, 106, 4181-4191, (2002).

Perry, M., Newman, J. and Cairns E., *Mass Transport in Gas-Diffusion Electrodes: A Diagnostic Tool for Fuel-Cell Cathodes*, Journal of the Electrochemical Society, 145(1), (1998).

Pharoah, J., Karan, K., Sun, W., *On effective transport coefficients in PEM fuel cell electrodes: Anisotropy of the porous transport layers*, Journal of Power Sources, 161, 214-224, (2006).

Pour, V. and Kadlec, B., *Isothermal Effectiveness Factor of a Half-Order Reaction in a Spherical Particle*, Collection Czechoslov. Chem Commun, 33, 2706-2708, (1968).

Solartron Analytical, www.solartronanalytical.com/products/index.htm, (2008).

SGL Group: The Carbon Company Carbon, www.sglcarbon.com, (2008).

Shah, A.A., Kim, G-S., Sui, P.C., and Harvey, D., *Transient non-isothermal model of a polymer electrolyte fuel cell*, Journal of Power Sources, 163, 793-806, (2007).

Siegel, N.P., Ellis, M.W., Nelson, D.J. and Spakovský, M.R., *Single domain PEMFC model based on agglomerate catalyst geometry*, Journal of Power Sources, 115, 81-89, (2003).

Springer, T.E., Zawodzinski, T.A., and Gottesfeld, S., *Polymer electrolyte fuel cell model*, Journal of Electrochemical Society, 138(8), 2334-2342, (1991).

Springer, T.E, Wilson, M.S. and Gottesfield, S., *Modeling and Experimental Diagnostics in Polymer Electrolyte Fuel Cells*, Journal of Electrochemical Society., Vol. 140(12), 3513-3526, (1993).

Sun, W., Peppley, B. and Karan, K, *An improved two-dimensional agglomerate cathode model to study the influence of catalyst layer structural parameters*, Electrochimica Acta, 50, 3359-3374, (2005a).

Sun, W., Peppley, B. and Karan, K., *Modeling the influence of GDL and flow-field plate parameters on the reaction distribution in the PEMFC cathode catalyst layer*, Journal of Power Sources, 144, 42-53, (2005b).

Thiele, E.W., *Relationship Between Catalytic Activity and Size of Particle*, Ind. Eng. and Chem., 31(7), 916-920, (1939).

Wang, Q., Eiklerling, M., Song, D. and Lui, Z., *Structure and performance of differenet types of agglomerates in cathode catalyst layers in PEM fuel cells*, J Electroanal. Chemistry, 573, 61-69, (2004a).

Wang, Y. and Wang, C-Y., *A nonisothermal, two-phase model for polymer electrolyte fuel cells*, Journal of the Electrochemical Society, 153(6), A1193-A1200, (2006).

West, A. and Fuller, T., *Influence of rib spacing in proton-exchange membrane electrode assemblies*, Journal of Applied Electrochemistry 26(6), 557-565, (1996).

Wilke, C. R., 1950, Diffusional Properties of Multicomponent Gases, Chem. Eng. Prog., 46, 95-104.

Williams, M.V., et. al., *Characteristics of gas diffusion layers for PEMFC*, Journal of Electrochemical Society, 151, A1173-A1180, (2005).

Zhou, T. and Lui, H., *Effects of the electrical resistances of the GDL in a PEM fuel cell*, Journal of Power Sources, 161, 444-453, (2006).

Appendix A

Mesh and solver settings for the half-order reaction model are listed in the Tables below. This simulation case was run with an adaptive mesh at only one NCO (0.30V). Settings for both the stationary and parametric solver are given.

Table A.1: Model solver settings

Parameter	Value
Pivot threshold	0.1
Memory allocation factor	0.7

Table A.2: Stationary solver settings

Parameter	Value
Linearity	Automatic
Relative tolerance	1.0E-6
Maximum number of iterations	999
Manual tuning of damping parameters	Off
Highly nonlinear problem	Off
Initial damping factor	1.0
Minimum damping factor	1.0E-4
Restriction for step size update	10.0

Table A.3: Parametric solver settings

Parameter	Value
Parameter name	NCO
Parameter values	0.3
Predictor	Linear
Manual tuning of parameter step size	Off
Initial step size	0.0
Minimum step size	0.0
Maximum step size	0.0

Table A.4: Model adaptive mesh settings

Parameter	Value
Use adaptive mesh refinement in geometry	Current geometry
Maximum number of refinements	3
Maximum number of elements	10000000
Refinement method	Longest
Residual order	0
Weights for eigenmodes	1
Scaling factor	1
Stability estimate derivative order	2
Element selection method	Rough global minimum
Increase number of elements by	1.8
Worst element fraction	0.5
Element fraction	0.5

Appendix B

This appendix provides information about the PEMFC cathode equations solved by COMSOLTM to produce the figures in this thesis.

2D Cathode model – first order reaction

Porous Transport Layer

1. COMSOLTM computes the molar concentrations, c_{O_2} , c_{H_2O} , c_{N_2} and the potential, ϕ_e , in the PTL, from the transport equations below. There are no sink and source terms because no reaction takes place. Ionic transport is not present in the PTL. No-flux conditions are set at the land for gaseous species and at the channel for electronic species, as well as the cathode walls for all species. The initial concentrations at the channel PTL boundary are $c_{N_2} = 35.34$, $c_{O_2} = 9.18$, $c_{H_2O} = 6.97 \text{ mol/m}^3$. The electronic potential at the land/PTL interface is set as 0 V.

$$\begin{aligned}\nabla \cdot j_{O_2,P} &= \nabla \cdot (-D_{O_2m,P} \nabla c_{O_2}) = 0 \\ \nabla \cdot j_{H_2O,P} &= \nabla \cdot (-D_{H_2Om,P} \nabla c_{H_2O}) = 0 \\ \nabla \cdot j_{N_2,P} &= \nabla \cdot (-D_{N_2m,C} \nabla c_{N_2}) = 0\end{aligned}\tag{30}$$

$$\nabla \cdot i_{e,C} = -\nabla \cdot (k_{e,C} \nabla \phi_{e,local,C}) = 0\tag{31}$$

Catalyst Layer

1. Calculate the reaction rate constant, k_c . η_{local} is the difference between the local ionic and electronic potential in the catalyst layer. The initial guesses for the potentials, everywhere in the catalyst layer, are set at 0.05 V and 0 V, respectively. The local concentration overpotential, η_{conc} is subtracted from the local overpotential. The initial guess for the oxygen concentration is 9.18 mol/m³.

$$k_c = \frac{a_{Pt}^{eff} i_0^{ref}}{4F(1-\varepsilon_{CAT})C_{O2}^{ref}} \left[\exp\left(-\frac{\alpha_c nF}{RT}(\eta_{local} - \eta_{conc})\right) - \exp\left(\frac{(1-\alpha_c)nF}{RT}(\eta_{local} - \eta_{conc})\right) \right] \quad (32)$$

$$\eta_{conc} = -\frac{RT}{4F} \ln\left(\frac{C_{O2}}{C_{O20}}\right) \quad (33)$$

2. Determine the Thiele Modulus and effectiveness factor from the reaction rate constant.

$$\Phi_L = \frac{r_{agg}}{3} \sqrt{\frac{k_c}{D^{eff}}} \quad (34)$$

$$E_r = \frac{1}{\Phi_L} \left(\frac{1}{\tanh(3\Phi_L)} - \frac{1}{3\Phi_L} \right) \quad (35)$$

3. Calculate the source terms for each transport equation in the catalyst layer.

Oxygen	$\frac{y_{O_2}P}{H} \left(\frac{1}{E_r k_c (1 - \varepsilon_{CAT})} + \frac{(r_{agg} + \delta)\delta}{Da_{agg} r_{agg}} \right)^{-1}$
Water	$2 \times (1 + 2\alpha) \frac{y_{O_2}P}{H} \left(\frac{1}{E_r k_c (1 - \varepsilon_{CAT})} + \frac{(r_{agg} + \delta)\delta}{Da_{agg} r_{agg}} \right)^{-1}$
Nitrogen	-
Electrons	$4F \frac{y_{O_2}P}{H} \left(\frac{1}{E_r k_c (1 - \varepsilon_{CAT})} + \frac{(r_{agg} + \delta)\delta}{Da_{agg} r_{agg}} \right)^{-1}$
Protons	$4F \frac{y_{O_2}P_{O_2}}{H} \left(\frac{1}{E_r k_c (1 - \varepsilon_{CAT})} + \frac{(r_{agg} + \delta)\delta}{Da_{agg} r_{agg}} \right)^{-1}$

4. COMSOL™ computes the molar concentrations, c_{O_2} , c_{H_2O} , c_{N_2} and the potentials, Φ_p and Φ_e from the transport equations below. The sink and source terms are obtained from the above table. No-flux conditions are set at the catalyst layer/membrane interface for each gaseous species and for electrons. The ionic potential at this interface is set at the NCO.

$$\begin{aligned}\nabla \cdot j_{O_2,C} &= \nabla \cdot (-D_{O_2m,C} \nabla c_{O_2}) = S_{O_2,C} \\ \nabla \cdot j_{H_2O,C} &= \nabla \cdot (-D_{H_2Om,C} \nabla c_{H_2O}) = S_{H_2O,C} \\ \nabla \cdot j_{N_2,C} &= \nabla \cdot (-D_{N_2m,C} \nabla c_{N_2}) = 0\end{aligned}\quad (36)$$

$$\nabla \cdot i_{p,C} = -\nabla \cdot (k_p \nabla \phi_{p,local,C}) = S_{p,C} \quad (37)$$

$$\nabla \cdot i_{e,C} = -\nabla \cdot (k_{e,C} \nabla \phi_{e,local,C}) = S_{e,C} \quad (38)$$

5. COMSOL™ solves the equations in steps 1 through 4 iteratively until convergence.

2D Cathode model – half-order reaction

Porous Transport Layer

Same equations as the first-order reaction.

Catalyst Layer

1. Calculate the reaction rate constant, k_c .

$$k_c = \frac{a_{Pt}^{eff} i_0^{ref}}{4F(1-\varepsilon_{CAT})(C_{O2}^{ref})^{0.5}} \left[\exp\left(-\frac{\alpha_c nF}{RT}(\eta_{local} - \eta_{conc})\right) - \exp\left(\frac{(1-\alpha_c)nF}{RT}(\eta_{local} - \eta_{conc})\right) \right] \quad (39)$$

$$\eta_{conc} = -\frac{RT}{4F} \ln\left(\frac{c_{O2}}{c_{O20}}\right) \quad (40)$$

2. Determine the Thiele Modulus and effectiveness factor from the reaction rate constant.

$$\Phi_L = \frac{r_{agg}}{3} \sqrt{\frac{k_c}{(C_{O2,l/s})^{0.5} D^{eff}}} \quad (41)$$

$$E_r = \frac{3.46}{\Phi} - \frac{3.30}{\Phi^2} - \frac{1.485}{\Phi^3} \quad \Phi > 4 \quad (42)$$

$$E_r = 1 - \frac{1}{30} \Phi^2 + \left(\frac{-3}{3780} + \frac{3}{1890} \right) \Phi^4 \quad \Phi < 4 \quad (43)$$

3. Calculate the source terms for each transport equation in the catalyst layer. The molar flux, j_{O2} is solved for using the quadratic equation.

Oxygen	$j_{O2} = \frac{r_{agg} Da_{agg}}{(r_{agg} + \delta)\delta} \left(C_{O2,g/l} - \frac{(j_{O2})^2}{[4FE_r k_c (1 - \varepsilon_{cat})]^2} \right)$
Water	$2 \cdot (1 + 2\alpha) \cdot j_{O2}$
Nitrogen	-
Electrons	$4F \cdot j_{O2}$
Protons	$4F \cdot j_{O2}$

4. COMSOLTM computes the molar concentrations, c_{O2} , c_{H2O} , c_{N2} and the potentials, Φ_p and Φ_e from the transport equations below. The sink and source terms are obtained from the above table. No-flux conditions are set at the catalyst layer/membrane interface for each gaseous species and for the electrons. The ionic potential at this interface is set at the NCO.

$$\begin{aligned} \nabla \cdot j_{O2,C} &= \nabla \cdot (-D_{O2m,C} \nabla c_{O2}) = S_{O2,C} \\ \nabla \cdot j_{H2O,C} &= \nabla \cdot (-D_{H2Om,C} \nabla c_{H2O}) = S_{H2O,C} \\ \nabla \cdot j_{N2,C} &= \nabla \cdot (-D_{N2m,C} \nabla c_{N2}) = 0 \end{aligned} \quad (44)$$

$$\nabla \cdot i_{p,C} = -\nabla \cdot (k_p \nabla \phi_{p,local,C}) = S_{p,C} \quad (45)$$

$$\nabla \cdot i_{e,C} = -\nabla \cdot (k_{e,C} \nabla \phi_{e,local,C}) = S_{e,C} \quad (46)$$

5. COMSOLTM solves the equations in steps 1 through 4 iteratively until convergence